Wintertime Southern Hemisphere jet streams shaped by interaction of transient eddies with Antarctic orography.

Matthew Patterson*, Tim Woollings and Neil T. Lewis

Atmospheric, Oceanic and Planetary Physics, University of Oxford, UK

Thomas Bracegirdle

British Antarctic Survey, Cambridge, UK

Corresponding author address: Matthew Patterson, Atmospheric, Oceanic and Planetary Physics, University of Oxford, Oxford, UK

E-mail: matthew.patterson@physics.ox.ac.uk

ABSTRACT

The wintertime Southern Hemisphere extratropical circulation exhibits considerable zonal asymmetries. We investigate the roles of various surface boundary conditions in shaping the mean state using a semi-realistic, atmosphere-only climate model. We find, in agreement with previous literature, that tropical sea surface temperature (SST) patterns are an important contributor to the mean state, while mid-latitude SSTs and sea ice extent play a smaller role. Our main finding is that Antarctic orography has a first order effect on the structure of the mid-latitude circulation. In the absence of Antarctic orography, equatorward eddy momentum fluxes associated with the orography are removed and hence convergence of eddy momentum in mid-latitudes is reduced. This weakens the Indian Ocean jet, making Rossby wave propagation downstream to the South Pacific less favourable. Consequently the flow stagnates over the mid to high-latitude South Pacific and the characteristic split jet pattern is destroyed. Removing Antarctic orography also results in a substantial warming over East Antarctica partly because transient eddies are able to penetrate further polewards, enhancing poleward heat transport. However, experiments in which a high latitude cooling is applied indicate that these temperature changes are not the primary driver of circulation changes in mid-latitudes. Instead, we invoke a simple barotropic mechanism in which the orographic slope creates an effective potential vorticity gradient which alters the eddy momentum flux.

1. Introduction

Many of the key zonal mean features of the Earth's atmospheric circulation, such as eddy-driven jets and Hadley cells, can be understood under zonally symmetric surface boundary conditions. Time-mean zonal asymmetries to the atmospheric flow can then largely be explained by the addition of zonally varying sea surface temperatures (SSTs), land-sea contrasts and orography (e.g. Wang and Ting 1999; Held et al. 2002; Brayshaw et al. 2009, 2011). The atmospheric circulation of the Southern Hemisphere (SH) during winter is notably asymmetric and characterised by an upper level jet spiraling in towards Antarctica (Hoskins and Hodges 2005; Williams et al. 2007). This can be seen in figure 1, plotted using winter (June, July and August - JJA) ERA-Interim reanalysis data for the years 1979-2014. A strong mid-latitude jet exists over the Indian Ocean which subsequently bifurcates into subtropical and polar branches, forming the so-called 'split jet' over the South Pacific (e.g. van Loon et al. 1972; Karoly and Vincent 1998; Bals-Elsholz et al. 2001). This behaviour contrasts strongly with the summer season, in which the atmospheric circulation is largely zonally symmetric.

Inatsu and Hoskins (2004) performed a set of atmosphere-only general circulation model (AGCM) experiments, in which they removed various aspects of the surface boundary conditions which may contribute to the structure of the SH winter storm tracks. In particular, they removed orography from Southern Africa and South America and set SSTs to the zonal mean in the tropics and mid-latitudes. They concluded that zonal asymmetries in tropical SSTs were responsible for most of the large-scale structure in mid-latitudes. They suggested that convection related to the Asian monsoon triggers a stationary Rossby wave which propagates south-east towards the South Pacific creating the split in the flow.

A distinct, but complementary perspective on the split jet centres around the strengthening of the subtropical jet in late spring (Williams et al. 2007; Nakamura and Shimpo 2004). The subtropical jet is driven by angular momentum transport via the Hadley cell and acts as a strong wave-guide for mid-latitude eddies, suppressing the eddy-mean flow feedback of the poleward eddy-driven jet (Nakamura and Shimpo 2004). That is, upper level eddies forming upstream over the Indian Ocean become trapped by the subtropical jet and are separated in latitude from the region of maximum baroclinicity at the surface (Nakamura and Sampe 2002). The upper level eddies are unable to interact with the surface baroclinic zone, suppressing wave activity and hence reducing the number of meridionally propagating eddies which provide the momentum source for the eddy-driven jet. However, sufficient upper level eddy activity persists at high latitudes to maintain a weak polar jet and hence a split jet is observed.

On the other hand, Ogawa et al. (2016) emphasised the importance of the mid-latitude SST front location in maintaining the split jet. The SST front determines the region of maximum baroclinicity and thus is the source region of transient eddies which provide the momentum driving the eddy-driven jet. They argued that a split jet forms over the South Pacific because there is sufficient separation in latitude between the mid-latitude SST front (approx. 55S) and the subtropical jet for a poleward eddy-driven jet to form. This contrasts with the Indian Ocean as the SST front formed by the Agulhas current is located further equatorwards (approx. 40S) and there is no splitting of the atmospheric flow.

Additionally, a significant perturbation to the SH circulation is provided by Antarctica. The year-round presence of snow and ice keeps the air above cold, maintaining a strong equator-to-pole temperature contrast. Moreover, much of the Antarctic continent is covered with over 3km of ice and the presence of this orography enhances longwave cooling to space (Ogura and Abe-Ouchi 2001; Singh et al. 2016), further cooling the surface. Longwave cooling at the top of the

Plateau drives a strong and relatively persistent drainage flow which is sharply constrained by topography (Parish and Bromwich 2007). The drainage flow is fed by a meridional overturning circulation which rises between 60S and 70S, moves polewards at upper levels and subsides over the continent (Parish and Bromwich 2007). Whilst the overturning circulation is thermally direct, eddy fluxes of momentum and heat are necessary to maintain the balance with the easterly Coriolis torque (Juckes et al. 1994).

Several studies have examined the effect of removing Antarctic orography on high-latitude climate. Some consistent findings have included an increase in poleward heat flux (Mechoso 1980, 1981; Parish and Bromwich 2007; Quintanar and Mechoso 1995; Walsh et al. 2000; Ogura and Abe-Ouchi 2001; Singh et al. 2016), an increase in poleward momentum flux (Egger 1991; Parish et al. 1994; Singh et al. 2016) and a reduction in high latitude cyclogenesis (Mechoso 1980; Simmonds and Law 1995; Walsh et al. 2000). Additionally, Lachlan-Cope et al. (2001) noted that the Antarctic Plateau is displaced by over 10° from the South Pole, resulting in a significant non-axisymmetric perturbation to the flow. Using AGCM experiments they found that the displacement of the orography is responsible for the existence of the Amundsen Sea Low, a highly variable region of sea level pressure near the West Antarctic coastline. It is clear that Antarctic orography influences the circulation at high latitudes, but how much of a role does it play in shaping the flow in the mid-latitudes?

In this study we build on the work of Inatsu and Hoskins (2004) and investigate the influence that altering various surface boundary conditions has on the zonally asymmetric structure of the SH wintertime circulation. We particularly consider the importance of Antarctic orography for the configuration of jet streams and demonstrate that without the Plateau, the split jet does not form over the South Pacific.

In section 2 the model and experiments are described followed by a comparison of the CONTROL experiment with ERA-Interim reanalysis in section 3. The circulation in each of the model runs is then discussed in section 4 before going into more depth on the role of Antarctic orography in section 5. Subsequently, in section 6 a barotropic model is employed to explain some of the effects of orography on circulation and conclusions are given in section 7.

2. Data and methodology

Isca

For this study we perform a set of idealised AGCM experiments using the modelling framework, Isca (Vallis et al. 2018). Our CONTROL experiment is broadly similar to the setup used by Thomson and Vallis (2018) except we use prescribed SSTs rather than a slab ocean. The model integrates the primitive equations using a spectral dynamical core with 40 levels in the vertical and at T42 horizontal resolution. This translates to a grid-point spacing of approximately 2.8° at the equator.

Water vapour is represented in the model atmosphere; its interactions with the atmosphere and surface by means of latent heating effects are included, and it is advected with the flow. Evaporation of water vapour occurs at the surface, and is parameterised as in Frierson et al. (2006) and Thomson and Vallis (2018). Here, the evaporative resistance parameter is given a value of 1.0 over the land and 0.7 for the sea surface, following Thomson and Vallis (2018). The 'fast' condensation of water vapour, whereby water vapour is removed as precipitation that reaches the surface immediately, occurs aloft. This treatment of condensation means that there is no explicit liquid water content in the model atmosphere, and thus by extension, no representation of clouds (Vallis et al. 2018). Precipitation may occur due to large-scale condensation within a grid box, or

moist convection. Large-scale condensation is parameterised following Frierson et al. (2006), and moist convective adjustment is parameterised following Betts and Miller (1986).

Radiative transfer is represented using the RRTM multi-band radiation scheme (Clough et al. 2005). Water vapour in the model atmosphere is radiatively active at long- and short-wavelengths. The carbon dioxide concentration is kept fixed at 350ppmv, and the zonal mean ozone concentration is set at 1990 levels. Surface albedo values are set to 0.25 for ocean, 0.325 for land and 0.7 for ice, following Thomson and Vallis (2018). These choices account for the absence of a cloud albedo contribution, and yield a planetary albedo of 0.31 which is comparable to the value of 0.29 calculated for the real Earth system (Stephens et al. 2015). The effect of ice on the atmosphere is primarily distinguished from that of land and SSTs by its higher albedo.

To include the effect of gravity wave drag on the upper stratosphere, Rayleigh damping with a timescale of 0.5 days is applied in a sponge layer above 1.5hPa, similar to Polvani and Kushner (2002) and Jucker and Gerber (2017). However, sub-grid orographic effects and orographic gravity wave-drag are excluded from the model. The boundary layer is represented via a Monin–Obukhov scheme (Frierson et al. 2006) with the surface roughness parameter an order of magnitude higher over land (values again follow Thomson and Vallis 2018).

In terms of surface boundary conditions, the same SSTs and ice fraction as used for AMIP (Taylor et al. 2000) are averaged for each month of the year to produce a monthly varying climatology, which is then used to force the model. Any grid box with an ice fraction of 50% or greater has its albedo set to the ice albedo value (0.7). The low horizontal resolution means that the model will not fully capture sharp SST gradients (Brayshaw et al. 2008; Sampe et al. 2010). However as we will show, the model is able to represent the key features of the SH circulation relatively well and SST perturbations in our experiments are large and hence should be easily captured by the model

atmosphere. Finally, the land mask and topographic height field are both taken from ERA-Interim (Dee et al. 2011).

Model experiments

Following Inatsu and Hoskins (2004) we alter various boundary conditions and examine the impact of these changes on the atmospheric circulation. An obvious caveat is that the real atmosphere is coupled with the ocean, so in the real Earth system many of the changes imposed here may be mitigated by changes to ocean circulation. Indeed, Singh et al. (2016) emphasised that including an ocean model reduces the change in atmospheric energy transport upon flattening Antarctica, with the largest reduction occurring in the tropics (their figure 4). However, our focus is on mid to high-latitudes where the change is less significant. Imposing different boundary conditions at the surface also allows us to draw more conclusions about the causality of changes in the model.

A CONTROL experiment is integrated for 30 model years with the first two years taken as spin-up. As in Inatsu and Hoskins (2004), we perform a run with SSTs between 20N and 20S set to the zonal mean and a run with SSTs south of 35S set to the zonal mean. These are respectively labelled ZTS and ZMS. The SST patterns for both of these runs are shown in figure 2, along with the region of high SST gradients. It is clear that in the ZMS run, the mid-latitude SST gradients are substantially diminished. In order to test the sensitivity of the jet latitude to the latitude of the sea ice edge, we retreat the sea ice edge back to the edge of the land mass calling this run NSI (figure 2d). In regions where sea ice is removed, the SSTs are taken to be 273K. Finally, to test the role of Antarctic orography in SH circulation, we run the model with Antarctic orography removed. Figure 2e shows the CONTROL orography contoured every 500m. The height and steepness of surface elevation are most significant over East Antarctica where it rises steeply from the coast to over 3000m above sea level. We create two runs without Antarctic orography, the first

with SSTs as in the CONTROL (NOROG) and the second with the same SSTs as in the ZTS run (NOROG_ZTS). A summary of the model boundary conditions for each run is given in table 1.

3. Comparison of the CONTROL run with ERA-Interim reanalysis

The experiments that we perform are idealised, however we still require that the model CONTROL run represents the atmosphere sufficiently well for our results to map onto the real Earth system. Figure 3 shows a comparison of the JJA zonal mean temperature and zonal mean zonal wind between the CONTROL run and ERA-Interim. Much like coupled climate models in CMIP5 (Taylor et al. 2012), the model extratropical troposphere is cold-biased and the jet is overly equatorward (Bracegirdle et al. 2013; Simpson et al. 2014; Lee 2015). The temperature bias has a magnitude of around 1-2K in most of the troposphere, but is substantially higher in the lower stratosphere, reaching 9K. It is likely that the lack of gravity wave drag in the model's lower stratosphere contributes to these biases (e.g. McFarlane 1987). With respect to the zonal wind structure, the mid-latitude jet over the Indian Ocean is too strong and equatorwards, while the polar front jet over the South Pacific is too weak, the latter being a result found in many CMIP5 models (Bracegirdle et al. 2013; Arakelian and Codron 2012; Patterson et al. 2019). However, the model is here being used for a rather idealised study and we conclude that it represents the SH circulation well enough for our purposes.

4. Tropical SST asymmetries and stationary Rossby waves

The key result of Inatsu and Hoskins (2004) was that the observed stationary wave pattern and much of the zonally asymmetric structure to the SH winter circulation is forced by tropical SST asymmetries. In order to show that this is reproduced in our experiments, we now plot the 300hPa stationary eddy stream function, $\psi*$, calculated as the zonally asymmetric component of

the stream function, along with wave activity flux vectors (Takaya and Nakamura 1997, 2001), W, in figure 4. The horizontal components of wave activity flux are calculated as follows,

$$W = \frac{p}{p_0}\begin{bmatrix} \frac{\partial\overline{\psi*}}{\partial x}\frac{\partial\overline{\psi*}}{\partial x} - \overline{\psi*}\frac{\partial^2\overline{\psi*}}{\partial x^2} \\ \frac{\partial\overline{\psi*}}{\partial x}\frac{\partial\overline{\psi*}}{\partial y} - \overline{\psi*}\frac{\partial^2\overline{\psi*}}{\partial x\partial y} \end{bmatrix},$$

in which p is the pressure level, p_0 is the surface pressure and overbars indicate the time-mean. We use monthly-mean data for this plot to isolate the stationary wave activity flux. The CONTROL run (figure 4a) is dominated by zonal wavenumber 1 waves with wave activity propagating south-eastwards from the Indian Ocean and refracting equatorwards to the east of the dateline. A comparison of the stationary wave patterns in CONTROL with ERA-Interim is shown in figure S1 of the supplementary material. The patterns are similar, though the stationary wave has a slightly higher amplitude in CONTROL than in reanalysis and the wave activity vectors to the south of Australia are orientated to the south-east rather than eastwards. In most of the runs this pattern of wave propagation remains largely the same as in CONTROL, however in agreement with Inatsu and Hoskins (2004) and Quintanar and Mechoso (1995), the stationary wave pattern and wave activity flux is severely diminished in the runs with zonally symmetric SSTs in the tropics (4b and 4c). The stationary waves are more subtly modified by the removal of Antarctic orography (figure 4d) as the pattern of cyclonic and anticyclonic anomalies remains broadly the same, but the centre of action over the Indian Ocean is diminished and the wave activity flux is weakened. The Antarctic Plateau clearly does exert some influence on stationary wave propagation as the pattern of wave activity flux found in ZTS (figure 4b) is much weaker in ZTS_NOROG (figure 4c).

Figure 5 shows the 500hPa wind and provides a complementary picture to the stationary wave changes in figure 4. In spite of the changes to surface temperature gradients and thus local baroclinicity in the ZMS experiment (figure 5e), the circulation is relatively unchanged. This appears to contradict the results of Ogawa et al. (2016) who found considerable differences between runs

with and without strong SST gradients. However a key difference lies in the fact that Ogawa et al. (2016) modified SST gradients by changing the meridional structure of the zonal mean SST (see their figure 1), whereas in our experiments the zonal mean SST is preserved. In the latter case, the zonal mean temperature profile will be largely the same as in the CONTROL state, however in the former case this will change, altering the zonal mean winds in line with thermal-wind balance. Hence, it may be that some of the changes observed by Ogawa et al. (2016) relate more to the change in equator-to-pole temperature gradient than to local SST gradients. The NSI run (figure 5f) shows a slight weakening of the eddy-driven jet in the South-East Pacific, off the Antarctic peninsula. It is notable that the South Pacific jet in CONTROL is located at high latitudes where it may be affected by removal of the proximal sea ice edge. Plotting figure 5 with a higher contour interval also shows wind anomalies in the NSI run of about $-2ms^{-1}$ at all longitudes over the high latitude Southern Ocean (not shown). A change of this magnitude is similar to that found in other studies on the atmospheric impact of Antarctic sea ice loss (England et al. 2018; Ayres and Screen 2019). Given the current rate of warming, significant Antarctic sea ice reductions are to be expected by the end of this century, with substantial effects on the climate system (Collins et al. 2013). However, in this study we are concerned with the boundary conditions shaping the mean state and it is clear from this figure that flattening Antarctica and removing tropical SST asymmetries have a much larger impact on SH circulation than sea ice retreat, even if these changes are impossible on a human timescale.

As expected, the circulation in the ZTS run is much more zonally symmetric than CONTROL, with the subtropical jet no longer a distinct feature and hence the South Pacific split jet pattern is destroyed (figure 5b). However, the split jet pattern is also absent in the NOROG experiment, but for a different reason, as the high latitude winds over the South Pacific are severely weakened and the subtropical jet is enhanced (figure 5d). Over the South Pacific, the anomalies seen in

these two runs with respect to CONTROL are almost equal and opposite, though both runs show a weakening over the Indian Ocean. Close examination of zonal wind changes in the ZTS_NOROG run (figure 5c) reveals that the responses to removal of tropical SST asymmetries and flattening Antarctica, do not add linearly over the high latitude South Pacific. That is, taken individually, removing tropical SST asymmetries and flattening Antarctica are both associated with a reduction in the strength of high latitude westerlies over the South Pacific (figure 5b,d), but this is not the case in ZTS_NOROG (figure 5c). This non-linearity can also be seen in figure S2f in the supplementary materials, in which anomalies are plotted with respect to ZTS_NOROG. Note that this study does not assume linearity, rather, we are demonstrating that the observed structure is contingent upon certain key boundary conditions. Another way in which to view the non-linear behaviour is to say that removal of Antarctic orography has a larger impact on atmospheric circulation in the presence of a stationary wave induced by tropical SSTs. Regarding the cause of non-linearity, this requires either non-linear interaction between stationary wave patterns induced by tropical and high-latitude sources or that transient eddy momentum fluxes play an important role. Seeing that the ZMS and NSI runs do not differ as markedly from the CONTROL run and the role of tropical SST asymmetry has been extensively discussed elsewhere (e.g. Inatsu and Hoskins 2004, 2006), we now focus our attention on the runs without Antarctic orography.

5. Effects of removing Antarctic orography

Effect on temperature

Previous studies on the effect of removing Antarctic orography have shown that the surface and air temperatures at high latitudes increase when the Plateau is removed (Ogura and Abe-Ouchi 2001; Singh et al. 2016). Figure 6a, which shows the temperature difference between the NOROG

and CONTROL runs, illustrates this point. The largest changes to the zonal mean temperature occur below 500hPa (figure 6a). However, it is clear from figure 6c that there is a substantial zonal asymmetry to these temperature changes, with increases in 500hPa temperature of 6K over parts of East Antarctica and no significant change over West Antarctica. These regionally varying changes closely correspond with the changes to elevation between the NOROG and CONTROL runs (figure 2).

The temperature changes occur for two reasons. Firstly, in the absence of orography, the column of air is deepened and hence there is more mass to absorb longwave radiation from the surface. This in turn heats the atmosphere which re-emits and warms the surface. Secondly, the removal of the Plateau allows transient eddies, which would normally be confined to the coastline, to access the continent and hence transport heat from lower latitudes, balancing the enhanced loss of energy to space. It therefore appears that there are two main ways in which removal of the Antarctic Plateau could alter the circulation, namely effects relating directly to the removal of the orography and effects through changes to the temperature gradients at high southern latitudes.

To try and understand which of these effects is more important in explaining the circulation changes seen in figures 4e and 5e, we perform a run without the Antarctic orography, but imposing a cooling tendency at high latitudes. This cooling is designed to cancel the temperature effects of removing the Plateau. The cooling tendencies are calculated first by performing a run like NOROG, but with Newtonian relaxation of the temperature field south of 65S at all pressure levels, to a seasonally varying climatology calculated from CONTROL. For regions in the CONTROL run which are masked out by orography, we set the relaxation temperature to follow a dry adiabatic lapse rate to the surface. The Newtonian cooling tendencies saved from this run are then used to create a climatology. Finally, a run without the Plateau is performed with the seasonally varying cooling tendencies imposed, named COOL. The advantage of using this method is that it doesn't

damp out eddy activity at high latitudes as is the case in the Newtonian relaxation run. Figure 6b shows the temperature difference between NOROG and COOL which is similar to the difference between NOROG and CONTROL. The main difference is a cold anomaly in the lower stratosphere between 60S and 70S. The lower tropospheric temperature perturbation is of the same magnitude, with a peak of 6-7K. It should be noted that while only the zonal mean temperature difference between COOL and NOROG is shown, the applied cooling is substantially zonally asymmetric.

In figure 7, a comparison is made of the 500hPa zonal wind fields in CONTROL, NOROG and COOL. It is clear that even with strong cooling of polar temperatures, the wind change from the COOL run is very similar to NOROG (figure 7b,c). For instance in figure 7c, the weakening of the flow over the South Pacific region remains much the same, as does the strengthening of the flow near the East Antarctic coastline. It might be expected that cooling would increase the local baroclinicity and promote stronger winds, but this only occurs at high latitudes and the flow in the mid-latitudes remains severely weakened with respect to CONTROL. This indicates that the removal of the mechanical effects of the orography itself and the subsequent effects on eddy propagation are likely more important in altering the mid-latitude circulation than the associated temperature perturbation.

Effect on circulation

We have so far noted that the circulation changes associated with flattening Antarctic orography are zonally asymmetric, with significant weakening of zonal wind over the South Pacific (figure 5). However, following many of the previous papers which have studied the effect of Antarctic orography on circulation we start by focussing on the zonal mean.

In figure 8, we plot the zonal mean momentum flux, heat transport and kinetic energy, associated with transient eddies. In calculating each of these quantities, daily-mean u, v and T have each

been high pass filtered using a 10 day Lanczos filter (Duchon 1979), indicated by primes. At high latitudes the CONTROL run sees an equatorward flux of eddy momentum (figure 8a) which is absent in NOROG. The absence of this flux reduces the convergence of eddy momentum in mid-latitudes, hence the weakened mid-latitude winds in NOROG (figure 5d,7b), consistent with Singh et al. (2016). We suggest that the changes to high latitude eddy momentum flux are likely linked to the removal of the orographic slope and will investigate this further in section 6. High latitude eddy heat flux is enhanced in NOROG as eddies are no longer confined to the coastline around Antarctica (figure 8b). However, eddy heat flux is also reduced in mid-latitudes with respect to CONTROL, which is consistent with the decrease in eddy kinetic energy seen in figure 8c. The changes to mid-latitude heat flux are in contrast to Mechoso (1981), who found much more substantial increases in eddy heat flux associated with removing the Antarctic Plateau. We also plot eddy statistics for the COOL run, in which a high latitude cooling tendency has been applied. In this run, the poleward heat flux south of 60S is enhanced in comparison to NOROG, in order to balance the cooling (figure 8b). However, the COOL zonal mean momentum fluxes are almost identical to those of NOROG (figure 8a), consistent with the similar zonal wind climatologies in figure 7b,c. Interestingly, eddy kinetic energy is greater at high latitudes in NOROG and COOL than in CONTROL, even though the momentum flux is very weak there. It appears that even if the magnitude of high latitude eddy kinetic energy is lower in CONTROL, the eddies are more efficient at transporting momentum northward than in NOROG and COOL. A similar picture is seen in figure 9 with zonal wind and EP flux diagnostics (Edmon et al. 1980), which indicate the propagation of wave activity. EP flux is defined under the quasi-geostrophic approximation as

$$F = a\cos(\phi)\left(-[u^*v^*], f\frac{[v^*\theta^*]}{\theta_p}\right),$$

where u and v are respectively the daily zonal and meridional wind, f is the Coriolis parameter and θ the potential temperature. The radius of the Earth is a, while p and ϕ are the pressure and meridional co-ordinates. Square brackets represent the zonal mean, asterisks indicate departures from the zonal mean and θ_p is the derivative of the potential temperature climatology with respect to pressure. No filtering is applied to u and v in figure 9, though if a high pass filter is used the resulting figures are similar, whereas vectors are substantially diminished when using monthly-mean data. This indicates that transient eddies dominate the observed changes over stationary eddies. The vectors are plotted following the convention of Edmon et al. (1980).

In the CONTROL run, the zonal mean zonal wind peaks at around 50S in the lower troposphere and is close to zero over Antarctica. EP flux vectors indicate that waves propagate upwards in the lower troposphere and then mostly equatorwards, strengthening the surface westerlies and eddy-driven jet. On the poleward side of the jet, vectors are directed polewards suggesting an equatorward flux of momentum which helps to maintain the jet on the poleward side. In agreement with previous authors, flattening Antarctica increases the zonal mean zonal wind south of 65S and decreases it in mid-latitudes (Mechoso 1981; Singh et al. 2016). This is consistent with the fact that in NOROG, there is no equatorward momentum flux reinforcing the poleward flank of the jet (figure 8a).

However, the zonal mean masks the considerable zonal structure to the changes seen in figure 10. In the CONTROL run, 700hPa $v'T'$ is strongest over the Indian Ocean with weaker though still significant, heat transport at mid to high latitudes over the South Pacific. Without Antarctic orography, transient eddy heat transport is extended polewards over the South Atlantic and South Indian Oceans as in the zonal mean (figure 8b), but $v'T'$ is considerably diminished in the South Pacific region (figure 10b,c). Surprisingly, it thus appears that removal of the zonally asymmetric orography creates an even more asymmetric storm track. Figure 10 also shows horizontal E vectors

(Hoskins et al. 1983) which provide a useful measure of transient wave activity flux on a given pressure level. The westerly acceleration by transient eddies is proportional to the horizontal divergence of the E vectors in a given region. E vectors are defined as

$$E = \left(\overline{v'^2 - u'^2}, -\overline{u'v'} \right),$$

with primes again indicating that the data has been 10 day high pass filtered and over-bars representing time averages. As was the case with $v'T'$, wave activity is abruptly reduced over the high latitude South Pacific upon flattening Antarctica. The meridional component of E indicates the transient meridional flux of eddy momentum and this dominates the differences between the two runs at high latitudes (figure 10c), consistent with figures 8a and 9.

Thus far it has become clear that the largest mid-latitude circulation changes in response to flattening Antarctica, occur in the South Pacific region (figures 5,10), downstream of the most significant orography. In addition to the development of local instabilities, the eddies which reinforce the mean flow are often generated from further west by the process of downstream development (Chang and Orlanski 1993; Hoskins and Hodges 2005). To investigate the role that Rossby waves from upstream might play, we plot lagged correlations of meridional wind in figure 11 as in Chang (1993, 1999). A base-point is chosen (here 180E, 62S, indicated by the white cross) before correlations between 300hPa meridional wind at that point and meridional wind at 850hPa and 300hPa, at all other grid-points are calculated and plotted. In the CONTROL run, meridional wind anomalies over the South Pacific are associated with a Rossby wave train from the Indian Ocean. This initially propagates south-east and continues eastwards toward South America, refracting equatorwards past about 200E. Comparing correlations with 850hPa and 300hPa, there is a close correspondence between anomalies at the two levels, with a slight westward tilt with height indicating the wave has a small baroclinic component. In contrast to the clear Rossby wave train

in CONTROL, anomalies in the NOROG run are more localised. This absence of coherent wave activity over the South Pacific in NOROG is consistent with the weakened mid-latitude flow there (figure 5e). It is likely that the equatorward momentum flux on the poleward side of the jet seen in the CONTROL run (figures 8a, 9 and 10a,c), reinforces the jet and enables it to act as a waveguide for transient waves. Removing the orography removes this momentum flux, weakens the Indian Ocean jet and hence makes Rossby wave propagation into the South Pacific less favourable. This is consistent with Codron (2007), who found that South Pacific eddy forcing is strongly influenced by zonal wind anomalies upstream, over the Indian Ocean. We therefore suggest that the reduced transient eddy heat flux and weak E vectors seen over the South Pacific in figure 8b, are related to the decrease in wind strength upstream via reductions in downstream development.

6. A barotropic model of orographic effects on transient eddies

In the absence of Antarctic orography, the jet stream weakens substantially in the Indian Ocean region (figure 5e) with implications for the South Pacific downstream (figure 10). Our argument so far, concerning reductions in eddy momentum flux changing the circulation, has a degree of circularity to it. This is because the interaction between eddies and the mean flow is a two way process; eddies generate the mean winds and the mean winds alter eddy propagation and also affect eddy generation through baroclinic instability. We now suggest an explanation for the influence of orography on eddy momentum fluxes using a barotropic model with bottom orography, stirred over a range of wavenumbers. Using this model has the advantages that it is conceptually simple and allows a better understanding of causality, as the eddy momentum fluxes generate the zonal winds in this model, but the winds do not affect the stirring which generates the eddies. It is worth noting that the differing mean-wind profiles will have some effect on eddy propagation. However, the

key point is that the stirring itself has the same properties in each run meaning that any differences between runs can ultimately be attributed to the presence or absence of orography.

The model is the same as in Vallis et al. (2004) and Barnes and Hartmann (2011) with the exception that we allow the depth of the fluid layer to vary in the meridional direction. The result of this is to add another term to the barotropic vorticity equation which effectively modifies the planetary vorticity gradient along gradients of orography. The key idea is that the presence of an orographic slope at high southern latitudes means that meridional exchange of air masses across the orographic slope will result in a northward flux of vorticity / westerly momentum (e.g. James 1989; Egger 1991). That is, an air column moving southward will be squashed and by conservation of potential vorticity, will become more anticyclonic. Conversely, an air column moving northward will be stretched and thus become anomalously cyclonic. We will demonstrate this effect by comparing runs with and without high latitude orography and then explain how the northward vorticity flux is achieved.

We begin with a layer of fluid with depth, H and relative vorticity, ζ. We write the depth of the fluid as $H(\phi) = H_T - h_B(\phi)$ in which H_T is the height of the tropopause, set as 10km, and h_B is the bottom topography. Potential vorticity, P is given by the following,

$$P = \frac{\zeta + f}{H},$$

as in Vallis (2017). Bottom topography is given a profile which is zero to the north of 65S and then slopes upward to a maximum at 90S. A cosinusoidal profile is used for the slope which is shown by a thick curve in figure 12c and mathematically described as follows

$$h_B(\phi) = \begin{cases} h_0 cos\left(\frac{90}{\phi_w}(\phi + 90)\right) & \phi \leq -90 + \phi_w \\ 0 & \phi > -90 + \phi_w, \end{cases}$$

with $\phi_w = 25^\circ$ and $h_0 = 3km$. The model is integrated on a sphere and takes the following form

$$\frac{\partial \zeta}{\partial t} + \frac{u}{a\cos\phi}\frac{\partial \zeta}{\partial \lambda} + \frac{v}{a}\frac{\partial \zeta}{\partial \phi} + \left(\beta + \frac{\zeta + f}{H}\frac{\partial h_B}{a\partial \phi}\right) v = S - r\zeta + \kappa\nabla^4\zeta,$$

where λ and ϕ are the zonal and meridional co-ordinates respectively. Similar to Vallis et al. (2004) and Barnes and Hartmann (2011), we apply stirring, S which parameterises baroclinic instability. S is an Ornstein-Uhlenbeck process defined as

$$S_{lm} = (1 - e^{2dt/\tau})^{1/2} Q^i + e^{-dt/\tau} S_{lm}^{i-1},$$

where l and m are respectively, the total and zonal wavenumber, dt is the timestep (900 seconds), i is an index for the current timestep and τ is a decorrelation timescale equal to 2 days. Q^i is a random number drawn from a uniform distribution in the range $[-7 \times 10^{-11}, 7 \times 10^{-11}]$. The stirring is only applied in mid-latitudes and this is achieved by multiplying S by a Gaussian function of half width 12°, centred on 45S. Linear Ekman damping is employed with coefficient, $r = \frac{1}{5} day^{-1}$ and the loss of vorticity at the smallest, unresolved scales is simulated via 4th order hyperdiffusion.

a. Barotropic model results

Like in the full Isca model, the barotropic model runs with and without orography are notably different in terms of momentum fluxes near the pole. Figure 12 shows the zonal mean zonal wind and transient eddy momentum transport, $u'v'$, in both models. In both Isca and barotropic runs, the model runs without orography (dashed curves) exhibit either weak or poleward momentum

fluxes at high latitudes in contrast to the runs with orography (solid curves), which show substantial equatorward momentum fluxes. In the latter cases this has a clear impact on the jet as the wind is reduced at high latitudes and enhanced in mid-latitudes. The Isca and barotropic runs without orography do differ in that momentum fluxes in the latter are positive (equatorward) at high latitudes, while momentum fluxes are negative (polewards) at all latitudes in the former. Previous studies have shown that flattening Antarctica results in enhanced baroclinic eddy growth at high latitudes (Simmonds and Law 1995; Walsh et al. 2000; Singh et al. 2016), consistent with the greater high latitude eddy kinetic energy in NOROG than in CONTROL (figure 10c). This provides a new source of eddy activity in NOROG, allowing equatorward momentum fluxes from higher latitudes than in CONTROL. This process is absent in the barotropic model runs. Note that in the Isca runs, momentum fluxes are shown at 300hPa as these are largest at this level, whereas winds are shown at 700hPa to isolate the eddy-driven jet (e.g. Woollings et al. 2010). We also define the effective planetary vorticity gradient as:

$$\beta_{eff} = \frac{2\Omega\cos(\phi)}{a} + \frac{\zeta + f}{H}\frac{\partial h_B}{a\partial\phi},$$

and plot this in figure 12c. This shows the sharp increase in the meridional vorticity gradient that the orography generates in the barotropic model.

The total wavenumber framework of Hoskins and Karoly (1981) is helpful here in understanding the propagation of waves and hence the momentum fluxes which generate the mean flow. The total wavenumber, K^*, is given by

$$K^* = \cos(\phi)\left(\frac{\beta - \frac{\partial^2 u}{\partial y^2}}{\overline{u} - c}\right)^{\frac{1}{2}},$$

in which $\overline{u} - c$ is the zonal mean zonal wind minus the wave phase speed. In general, waves propagate towards higher K^* until they encounter a turning latitude, where $K^* = k$, or a critical latitude, $\overline{u} = c$, at which K^* becomes infinite and simple barotropic wave theory breaks down, sometimes associated with non-linear wave-breaking (Hoskins and Ambrizzi 1993). We replace β with β_{eff} as defined above, in our definition of K^*, to account for the additional orographic β effect. Hence K^* becomes

$$K^* = \cos(\phi) \left(\frac{\beta_{eff} - \frac{\partial^2 u}{\partial y^2}}{\overline{u} - c} \right)^{\frac{1}{2}}.$$

In figure 13a, we see that without bottom orography, K^* generally decreases with increasing latitude and so any waves propagating polewards will tend to encounter a turning latitude and refract equatorwards, breaking in the subtropics. Hence the jet will mostly only be enhanced on its equatorward flank by eddy momentum fluxes. On the other hand, waves generated in mid-latitudes in the presence of high latitude orography, can also refract polewards towards higher K^*. For this reason, in this case, there will also be a significant equatorward momentum flux from high latitudes, in agreement with figure 12 and the full 3D model runs. The profile of K^* is partly shaped by the orographic β term, but the critical latitude at 65S is set by the latitude at which $\overline{u} = c$. Hence, the mean winds largely determine the propagation of transient eddies. However, it is worth emphasising that the only forcing difference that can lead to changes in the wind and the eddy fluxes between the runs with and without orography, is the orographic β term, $\frac{\zeta+f}{H}\frac{\partial h_B}{a\partial\phi}v$, as the eddy stirring is statistically identical. It can therefore be said that the increase in the jet speed is entirely due to the presence of high latitude orography.

In order to check that both Isca and the barotropic models are achieving momentum fluxes in a similar way, we plot correlations of meridional wind in figure 14, as in figure 11, but for the

base-point (110E, 62S) and at lag 0. This base-point is close to the most significant orography which rises steeply over East Antarctica. We also plot correlations for ERA-Interim to connect the results back to observational data. The two models show a remarkable correspondence for both experiments and the orography runs agree well with ERA-Interim.

For runs with orography, correlations show a Rossby wave train, centred on the base-point, with a distinctive southwest-northeast tilt to the positive meridional wind anomaly. This tilted pattern is characteristic of equatorward momentum flux. Downstream, the negative anomaly appears to follow the topographic gradient eastwards and remains at high latitudes. This is less obvious in the barotropic model (with orography), but is clearer at lags +1 and +2 (figures S4 and S5 of the supplementary material). The waves do not appear to break, but may be propagating along the effective potential vorticity gradient which results from the orographic slope (Egger and Fraedrich 1987). The tilt is caused by the propagation of eddies towards higher K^* as suggested by the poleward critical latitude in figure 13a. In contrast to these cases, the correlation patterns in runs without orography show a Rossby wave propagating south-eastwards from the west of the base-point, reaching the base-point and then refracting equatorwards. Whilst the waves exhibit a slight southwest-northeast tilt on reaching the base-point, the poleward momentum flux associated with the equatorward refraction cancels this out. Correlations for the runs without orography also appear to pick out a lower wavenumber. This is particularly the case when comparing the Isca runs, as the CONTROL has a typical wavenumber of 4-5 while NOROG exhibits a wavenumber of around 3-4. Typical wavenumbers of 4-5 at high latitudes in the CONTROL run are in agreement with the observational study of Chang (1999, his figure 3). Generally only the lowest wavenumber waves are able to propagate to high latitudes, but it is likely that the increase in potential vorticity gradient associated with orography allows waves of a higher wavenumber to reach polar latitudes.

In summary, when a high latitude orographic slope is imposed in a barotropic model with stochastic forcing, exchange of air masses across the orographic slope results in a vorticity flux away from the orography. In the steady state, transient eddies, generated by stirring in mid-latitudes, propagate towards a critical latitude which is set by the presence of high latitude easterlies along the orographic slope. The poleward propagation of eddies results in an equatorward momentum flux and thus the maintenance of a stronger eddy-driven jet. This is similar to the Indian Ocean sector where there is a steep orographic slope at high latitudes and a strong mid-latitude jet. Conversely, in the barotropic model run with no orography, waves encounter a turning latitude at high latitudes, preventing poleward wave propagation on the poleward side of the jet, consistent with lagged correlation plots in the Isca NOROG run (figure 14b).

7. Discussion and conclusions

In this study we have investigated the processes shaping the wintertime Southern Hemisphere circulation by altering various boundary conditions in an idealised model. In agreement with previous work, the structure of tropical SSTs was found to be critical for the formation of a quasi-stationary Rossby wave which creates the South Pacific split jet (Inatsu and Hoskins 2004, 2006). In contrast, removing the zonally asymmetric components of mid-latitude SST resulted in relatively weak changes to the overall circulation. Retreating sea ice back to the Antarctic continent also had a comparatively small impact on the circulation, though it did weaken the high latitude jet over the south-east Pacific. That is not to say that such changes would not have significant impacts on the climate system, but rather that mid-latitude SSTs and sea ice are not of first order importance in setting the mean atmospheric circulation in the SH.

In addition to tropical SSTs, we found the presence of orography over Antarctica to have a leading order effect on mid-latitude circulation. Without the Antarctic Plateau, eddy activity over

the Indian Ocean increased and was able to penetrate further polewards. However, high-latitude equatorward momentum fluxes also ceased, weakening the eddy driven jet. The largest changes occurred downstream in the South Pacific region as the storm track abruptly terminated over the Indian Ocean (illustrated by $v'T'$ in figure 10). Concomitantly, the mid to high latitude winds over the South Pacific severely weakened and the split jet was destroyed. Whilst idealised, these experiments illustrate the dependence of the wintertime South Pacific circulation on the flow upstream over the Indian Ocean (e.g. Chang 1999; Codron 2007). Propagation of Rossby waves from the Indian Ocean to the South Pacific became less favourable in the absence of Antarctic orography (figure 11), likely because of the weakening of the Indian Ocean jet, making it less effective as a waveguide (Hoskins and Ambrizzi 1993). These results appear all the more intriguing when considering that Antarctic orography is itself considerably zonally asymmetric, and yet removing this feature results in an even more zonally asymmetric atmospheric circulation. We also noted that circulation anomalies associated with removal of tropical SST asymmetries and anomalies associated with flattening Antarctica, do not add linearly when both changes are imposed in the same run (figure 5c). This non-linearity is particularly seen over the South Pacific and could be related to the dependence of the South Pacific on downstream propagation of transient Rossby waves, as discussed above.

Our results have broadly been in agreement with those of previous studies investigating the effect of Antarctic orography on circulation. For instance, we found a large warming at high latitudes and an increase in poleward heat flux at high latitudes upon flattening Antarctica (Mechoso 1981; Simmonds and Law 1995; Ogura and Abe-Ouchi 2001; Singh et al. 2016). At the same time, we found an increase in high latitude westerly winds and a decrease in wind strength in mid-latitudes (Mechoso 1981; Singh et al. 2016). Furthermore, we showed substantial zonal asymmetries to the mid-latitude circulation response, with the largest changes occurring in the South Pacific region,

a finding which was alluded to in Simmonds and Law (1995). However, in contrast to Simmonds and Law (1995), we have found that the temperature perturbation resulting from flattening Antarctica, is of lesser importance in determining changes to large-scale atmospheric dynamics (figure 7). Rather, we have shown that it is the presence of the orographic slope itself which altered the dynamics of eddies, increasing the convergence of eddy momentum in mid-latitudes. Flattening the orography in Isca enabled transient eddies to penetrate further south over the Antarctic continent, as measured in eddy kinetic energy and heat transport. Despite this, the eddy momentum fluxes over Antarctica are considerably stronger in the case with orography.

We have provided an explanation for this influence of Antarctic orography on mid-latitudes using a simple barotropic model with bottom topography varying in latitude. The effect of this was to add an additional orographic β term which modified high latitude eddy momentum fluxes, enhancing the eddy-driven jet in mid-latitudes. β is relatively weak at high latitudes (figure 12c), but as a result of the orographic β effect and changes to the zonal mean wind profile, it appears that waves tend to refract polewards towards the greater potential vorticity gradient (figure 14). The eddies thus exhibit a southwest-northeast tilt at high latitudes, which is effective at transporting momentum equatorwards, strengthening the jet. Whilst simplified, we have shown that the output of this model corresponds closely, at least in a qualitative sense, with effects seen in the full 3D model. We have also shown that the eddy tilt seen in the barotropic and 3D models is present in observations (figure 14). The importance of eddy momentum fluxes over Antarctica was also emphasised by Juckes et al. (1994). Surface cooling over the continent results in downslope winds from the centre of the continent towards the coast. The Coriolis torque acting on these generates surface easterly winds, and the drag on these constitutes a source of westerly momentum for the atmosphere over Antarctica. Equatorward transient eddy momentum fluxes play an important

role in balancing this source term, and our results suggest that eddy refraction by the orographic potential vorticity gradient is a key mechanism which provides these fluxes.

Many CMIP5 models struggle to capture the polar front branch of the South Pacific split jet seen in reanalysis data. The fine details of Antarctic orography may be smoothed out due to the coarse resolution of climate models, but the orographic effects on eddies that we have considered are unlikely to be sensitive to these details. However, the present study does suggest that both the strength of the wind and the nature of Rossby wave propagation over the Indian Ocean are important for the split jet. Consequently, we have shown that in order to correctly capture the South Pacific jet structure, a model must adequately capture the processes governing the upstream flow.

On paleo-timescales, Antarctic ice sheets have undergone considerable change and this is likely to have had a substantial effect on SH mid-latitude circulation. For example, Justino et al. (2014) performed simulations with Antarctic orography lowered by 25%, mimicking conditions in the mid to late Miocene (approx. 15 million years ago) and found weakened zonal mean zonal winds in mid-latitudes, consistent with the present study. However, it would be of interest to study the effect of altered Antarctic orography on SH circulation more systematically and quantitatively compare these changes with the effects of other long-term forcing variations such as changes to greenhouse gas concentrations and ocean circulation.

This work has concerned the asymmetry of the SH mean state, however studies have noted that the response of wintertime SH circulation under climate change is also considerably zonally asymmetric (Simpson et al. 2014; Grose et al. 2017; Patterson et al. 2019). It would be of interest to investigate which forcing mechanisms are responsible for driving these responses and how they relate to the mean state. The results of the present study lead us to speculate that changes to tropical SSTs are likely to be important, while sea ice retreat and mid-latitude SSTs are less likely to play a

major role in driving changes in the asymmetry. Indeed, several studies have shown links between observed high southern latitude circulation changes and tropical SST trends (Simpkins et al. 2014; Li et al. 2015). Our findings concerning the dependence of the South Pacific eddy-driven jet on the flow upstream are also relevant here, as any changes to the Indian Ocean region could potentially have an even greater impact on the Pacific.

Acknowledgments. We thank three anonymous reviewers for their comments and suggestions which improved the manuscript. We also thank Ronald Li and Chris O'Reilly for helpful discussions on this work. Finally, we thank ECMWF for the use of ERA-Interim reanalysis data, which was downloaded from the ECMWF website (https://www.ecmwf.int/en/forecasts/datasets/browse-reanalysis-datasets). Model data from the simulations in this study is available from the authors upon request. Matthew Patterson was funded by the Natural Environment Research Council (Grant NE/L002612/1).

References

Arakelian, A., and F. Codron, 2012: Southern Hemisphere Jet Variability in the IPSL GCM at Varying Resolutions. *Journal of the Atmospheric Sciences*, **69 (12)**, 3788–3799, doi:10.1175/JAS-D-12-0119.1, URL http://dx.doi.org/10.1175/JAS-D-12-0119.1.

Ayres, H., and J. Screen, 2019: Multimodel Analysis of the Atmospheric Response to Antarctic Sea Ice Loss at Quadrupled CO ₂. *Geophysical Research Letters*, **46 (16)**, 9861–9869, doi:10.1029/2019GL083653, URL https://onlinelibrary.wiley.com/doi/abs/10.1029/2019GL083653.

Bals-Elsholz, T. M., E. H. Atallah, L. F. Bosart, T. A. Wasula, M. J. Cempa, and A. R. Lupo, 2001: The wintertime southern hemisphere split jet: Structure, variability, and evolution. *Journal of*

Climate, **14 (21)**, 4191–4215, doi:10.1175/1520-0442(2001)014⟨4191:TWSHSJ⟩2.0.CO;2.

Barnes, E. A., and D. L. Hartmann, 2011: Rossby Wave Scales, Propagation, and the Variability of Eddy-Driven Jets. *Journal of the Atmospheric Sciences*, **68 (12)**, 2893–2908, doi:10.1175/JAS-D-11-039.1.

Betts, A. K., and M. J. Miller, 1986: A new convective adjustment scheme. Part II: Single column tests using GATE wave, BOMEX, ATEX and arctic air-mass data sets. *Quarterly Journal of the Royal Meteorological Society*, **112 (473)**, 693–709, doi:10.1002/qj.49711247308, URL http://doi.wiley.com/10.1002/qj.49711247308.

Bracegirdle, T. J., E. Shuckburgh, J. B. Sallee, Z. Wang, A. J. S. Meijers, N. Bruneau, T. Phillips, and L. J. Wilcox, 2013: Assessment of surface winds over the atlantic, indian, and pacific ocean sectors of the southern ocean in cmip5 models: Historical bias, forcing response, and state dependence. *Journal of Geophysical Research Atmospheres*, **118**, 547–562, doi:10.1002/jgrd.50153.

Brayshaw, D. J., B. Hoskins, and M. Blackburn, 2008: The Storm-Track Response to Idealized SST Perturbations in an Aquaplanet GCM. *Journal of the Atmospheric Sciences*, **65 (9)**, 2842–2860, doi:10.1175/2008JAS2657.1.

Brayshaw, D. J., B. Hoskins, and M. Blackburn, 2009: The Basic Ingredients of the North Atlantic Storm Track. Part I: Land–Sea Contrast and Orography. *Journal of the Atmospheric Sciences*, **66 (9)**, 2539–2558, doi:10.1175/2009JAS3078.1.

Brayshaw, D. J., B. Hoskins, and M. Blackburn, 2011: The Basic Ingredients of the North Atlantic Storm Track. Part II: Sea Surface Temperatures. *Journal of the Atmospheric Sciences*, **68 (8)**, 1784–1805, doi:10.1175/2011JAS3674.1.

Chang, E. K., 1993: Downstream development of baroclinic waves as inferred from regression analysis. *Journal of the Atmospheric Sciences*, **50 (13)**, 2038–2053, doi:10.1175/1520-0469(1993)050⟨2038:DDOBWA⟩2.0.CO;2.

Chang, E. K., and I. Orlanski, 1993: On the dynamics of a storm track. *Journal of the Atmospheric Sciences*, **50 (7)**, 999–1015, doi:10.1175/1520-0469(1993)050⟨0999:OTDOAS⟩2.0.CO;2.

Chang, E. K. M., 1999: Characteristics of Wave Packets in the Upper Troposphere. Part II: Seasonal and Hemispheric Variations. *Journal of the Atmospheric Sciences*, **56 (11)**, 1729–1747, doi:10.1175/1520-0469(1999)056⟨1729:COWPIT⟩2.0.CO;2, URL http://journals.ametsoc.org/doi/abs/10.1175/1520-0469{\%}281999{\%}29056{\%}3C1729{\%}3ACOWPIT{\%}3E2.0.CO{\%}3B2.

Clough, S. A., M. W. Shephard, E. J. Mlawer, J. S. Delamere, M. J. Iacono, K. Cady-Pereira, S. Boukabara, and P. D. Brown, 2005: Atmospheric radiative transfer modeling: A summary of the AER codes. *Journal of Quantitative Spectroscopy and Radiative Transfer*, **91 (2)**, 233–244, doi:10.1016/j.jqsrt.2004.05.058.

Codron, F., 2007: Relations between Annular Modes and the Mean State: Southern Hemisphere Winter. *Journal of the Atmospheric Sciences*, **64 (9)**, 3328–3339, doi:10.1175/JAS4012.1, URL http://journals.ametsoc.org/doi/abs/10.1175/JAS4012.1.

Collins, M., and Coauthors, 2013: Long-term Climate Change: Projections, Commitments and Irreversibility. *2013: Long-term Climate Change: Projections, Commitments and Irreversibility. In: Climate Change 2013: The Physical Science Basis. Contribution of Working Group I to the Fifth Assessment Report of the Intergovernmental Panel on Climate Change*, T. Stocker, D. Qin, G. K. Plattner, M. Tignor, S. Allen, J. Boschung, A. Nauels, Y. Xia, V. Bex, and Midgley. P.M., Eds., Cambridge University Press, chap. 12.

652 Dee, D. P., S. M. Uppala, A. J. Simmons, P. Berrisford, P. Poli, and S. Kobayashi, 2011: The ERA-
653 Interim reanalysis: Configuration and performance of the data assimilation system. *Quarterly*
654 *Journal of the Royal Meteorological Society*, **137 (656)**, 553–597, doi:10.1002/qj.828.

655 Duchon, C. E., 1979: Lanczos Filtering in One and Two Dimensions. *Journal of Applied Meteo-*
656 *rology*, **18**, 1016–1022.

657 Edmon, H. J., B. J. Hoskins, and M. E. McIntyre, 1980: Eliassen-Palm Cross Sections
658 for the Troposphere. *Journal of the Atmospheric Sciences*, **37 (12)**, 2600–2616, doi:
659 10.1175/1520-0469(1980)037⟨2600:EPCSFT⟩2.0.CO;2, URL http://journals.ametsoc.org/doi/
660 abs/10.1175/1520-0469{\%}281980{\%}29037{\%}3C2600{\%}3AEPCSFT{\%}3E2.0.
661 CO{\%}3B2.

662 Egger, J., 1991: On the mean atmospheric circulation over Antarctica. *Geophysical & As-*
663 *trophysical Fluid Dynamics*, **58 (1-4)**, 75–90, doi:10.1080/03091929108227332, URL http:
664 //www.tandfonline.com/doi/abs/10.1080/03091929108227332.

665 Egger, J., and K. Fraedrich, 1987: Topographic Rossby waves over Antarctica. *Tellus A*, **39A (2)**,
666 110–115, doi:10.1111/j.1600-0870.1987.tb00293.x, URL http://tellusa.net/index.php/tellusa/
667 article/view/11745.

668 England, M., L. Polvani, and L. Sun, 2018: Contrasting the Antarctic and Arctic atmospheric
669 responses to projected sea ice loss in the late twenty-first century. *Journal of Climate*, **31 (16)**,
670 6353–6370, doi:10.1175/JCLI-D-17-0666.1, URL www.ametsoc.org/PUBSReuseLicenses.

671 Frierson, D. M. W., I. M. Held, and P. Zurita-Gotor, 2006: A Gray-Radiation Aquaplanet
672 Moist GCM. Part I: Static Stability and Eddy Scale. *Journal of the Atmospheric Sciences*,

673 **63 (10)**, 2548–2566, doi:10.1175/JAS3753.1, URL http://journals.ametsoc.org/doi/abs/10.1175/
674 JAS3753.1.

675 Grose, M. R., J. S. Risbey, A. F. Moise, S. Osbrough, C. Heady, L. Wilson, and T. Erwin,
676 2017: Constraints on Southern Australian Rainfall Change Based on Atmospheric Circulation
677 in CMIP5 Simulations. *Journal of Climate*, **30 (1)**, 225–242, doi:10.1175/JCLI-D-16-0142.1,
678 URL http://journals.ametsoc.org/doi/10.1175/JCLI-D-16-0142.1.

679 Held, I. M., M. Ting, and H. Wang, 2002: Northern winter stationary waves: Theory and modeling.
680 *Journal of Climate*, **15 (16)**, 2125–2144, doi:10.1175/1520-0442(2002)015⟨2125:NWSWTA⟩
681 2.0.CO;2.

682 Hoskins, B. J., and T. Ambrizzi, 1993: Rossby Wave Propagation on a Realistic Longitudinally
683 Varying Flow. *Journal of the Atmospheric Sciences*, **50 (12)**, 1661–1671.

684 Hoskins, B. J., and K. I. Hodges, 2005: A new perspective on Southern Hemisphere storm tracks.
685 *Journal of Climate*, **18 (20)**, 4108–4129, doi:10.1175/JCLI3570.1.

686 Hoskins, B. J., I. N. James, and G. H. White, 1983: The Shape, Propagation and
687 Mean-Flow Interaction of Large-Scale Weather Systems. *Journal of the Atmospheric*
688 *Sciences*, **40 (7)**, 1595–1612, doi:10.1175/1520-0469(1983)040⟨1595:TSPAMF⟩2.0.CO;
689 2, URL http://journals.ametsoc.org/doi/abs/10.1175/1520-0469{\%}281983{\%}29040{\%
690 }3C1595{\%}3ATSPAMF{\%}3E2.0.CO{\%}3B2.

691 Hoskins, B. J., and D. J. Karoly, 1981: The Steady Linear Response of a Spherical Atmosphere
692 to Thermal and Orographic Forcing. *Journal of the Atmospheric Sciences*, **38 (6)**, 1179–1196,
693 doi:10.1175/1520-0469(1981)038⟨1179:TSLROA⟩2.0.CO;2.

Inatsu, M., and B. J. Hoskins, 2004: The zonal asymmetry of the Southern Hemisphere winter storm track. *Journal of Climate*, **17 (24)**, 4882–4892, doi:10.1175/JCLI-3232.1.

Inatsu, M., and B. J. Hoskins, 2006: The Seasonal and Wintertime Interannual Variability of the Split Jet and the Storm-Track Activity Minimum near New Zealand. *Journal of the Meteorological Society of Japan*, **84 (3)**, 433–445.

James, I. N., 1989: The Antarctic drainage flow: Implications for hemispheric flow on the Southern Hemisphere. *Antarctic Science*, **1 (3)**, 279–290, doi:10.1017/S0954102089000404.

Jucker, M., and E. P. Gerber, 2017: Untangling the Annual Cycle of the Tropical Tropopause Layer with an Idealized Moist Model. *Journal of Climate*, **30 (18)**, 7339–7358, doi:10.1175/JCLI-D-17-0127.1, URL http://journals.ametsoc.org/doi/10.1175/JCLI-D-17-0127.1.

Juckes, M. N., I. N. James, and M. Blackburn, 1994: The influence of Antarctica on the momentum budget of the southern extratropics. *Quarterly Journal of the Royal Meteorological Society*, **120 (518)**, 1017–1044, doi:10.1002/qj.49712051811, URL http://doi.wiley.com/10.1002/qj.49712051811.

Justino, F., J. Marengo, F. Kucharski, F. Stordal, J. Machado, and M. Rodrigues, 2014: Influence of Antarctic ice sheet lowering on the Southern Hemisphere climate: Modeling experiments mimicking the mid-Miocene. *Climate Dynamics*, **42 (3-4)**, 843–858, doi:10.1007/s00382-013-1689-9.

Karoly, D. J., and D. G. Vincent, 1998: *Meteorology of the Southern Hemisphere*. American Meteorological Society, 410 pp., doi:10.1007/978-1-935704-10-2.

Lachlan-Cope, T. A., W. M. Connolley, and J. Turner, 2001: The role of the non-axisymmetric Antarctic orography in forcing the observed pattern of variability of the Antarctic climate. *Geophysical Research Letters*, **28 (21)**, 4111–4114, doi:10.1029/2001GL013465.

Lee, R. W., 2015: Storm track biases and changes in a warming climate from an extratropical cyclone perspective using CMIP5. Ph.D. thesis, University of Reading.

Li, X., E. P. Gerber, D. M. Holland, and C. Yoo, 2015: A Rossby Wave Bridge from the Tropical Atlantic to West Antarctica. *Journal of Climate*, **28 (6)**, 2256–2273, doi:10.1175/JCLI-D-14-00450.1, URL http://journals.ametsoc.org/doi/10.1175/JCLI-D-14-00450.1.

McFarlane, N. A., 1987: The Effect of Orographically Excited Gravity Wave Drag on the General Circulation of the Lower Stratosphere and Troposphere. *Journal of the Atmospheric Sciences*, **44 (14)**, 1775–1800, doi:10.1175/1520-0469(1987)044⟨1775:TEOOEG⟩2.0.CO;2.

Mechoso, C. R., 1980: The Atmospheric Circulation Around Antarctica: Linear Stability and Finite-Amplitude Interactions with Migrating Cyclones. *Journal of the Atmospheric Sciences*, **37 (10)**, 2209–2233, doi:10.1175/1520-0469(1980)037⟨2209:TACAAL⟩2.0.CO;2, URL http://journals.ametsoc.org/doi/abs/10.1175/1520-0469{\%}281980{\%}29037{\%}3C2209{\%}3ATACAAL{\%}3E2.0.CO{\%}3B2.

Mechoso, C. R., 1981: Topographic Influences on the General Circulation of the Southern Hemisphere: A Numerical Experiment. *Monthly Weather Review*, **109 (10)**, 2131–2139, doi:10.1175/1520-0493(1981)109⟨2131:TIOTGC⟩2.0.CO;2, URL http://journals.ametsoc.org/doi/abs/10.1175/1520-0493{\%}281981{\%}29109{\%}3C2131{\%}3ATIOTGC{\%}3E2.0.CO{\%}3B2.

Nakamura, H., and T. Sampe, 2002: Trapping of synoptic-scale disturbances into the North-Pacific subtropical jet core in midwinter. *Geophysical Research Letters*, **29 (16)**, doi:10.1029/2002GL015535.

Nakamura, H., and A. Shimpo, 2004: Seasonal variations in the Southern Hemisphere storm tracks and jet streams as revealed in a reanalysis dataset. *Journal of Climate*, **17 (9)**, 1828–1844, doi:10.1175/1520-0442(2004)017⟨1828:SVITSH⟩2.0.CO;2.

Ogawa, F., H. Nakamura, K. Nishii, T. Miyasaka, and A. Kuwano-Yoshida, 2016: Importance of Midlatitude Oceanic Frontal Zones for the Annular Mode Variability: Interbasin Differences in the Southern Annular Mode Signature. *Journal of Climate*, **29 (17)**, 6179–6199, doi:10.1175/JCLI-D-15-0885.1, URL http://journals.ametsoc.org/doi/10.1175/JCLI-D-15-0885.1.

Ogura, T., and A. Abe-Ouchi, 2001: Influence of the Antarctic Ice Sheet on southern high latitude climate during the Cenozoic: Albedo vs topography effect. *Geophysical Research Letters*, **28 (4)**, 587–590, doi:10.1029/2000GL011366, URL http://doi.wiley.com/10.1029/2000GL011366.

Parish, T. R., and D. H. Bromwich, 2007: Reexamination of the Near-Surface Airflow over the Antarctic Continent and Implications on Atmospheric Circulations at High Southern Latitudes*. *Monthly Weather Review*, **135 (5)**, 1961–1973, doi:10.1175/MWR3374.1, URL http://journals.ametsoc.org/doi/abs/10.1175/MWR3374.1.

Parish, T. R., D. H. Bromwich, and Ren-Yow Tzeng, 1994: On the role of the Antarctic continent in forcing large-scale circulations in the high southern latitudes. *Journal of the Atmospheric Sciences*, **51 (24)**, 3566–3579, doi:10.1175/1520-0469(1994)051⟨3566:OTROTA⟩2.0.CO;2.

Patterson, M., T. Bracegirdle, and T. Woollings, 2019: Southern Hemisphere atmospheric blocking in CMIP5 and future changes in the Australia-New Zealand sector. *Geophysical Research Letters*, **46 (15)**, 9281–9290, doi:10.1029/2019GL083264, URL https://onlinelibrary.wiley.com/doi/abs/10.1029/2019GL083264.

Polvani, L. M., and P. J. Kushner, 2002: Tropospheric response to stratospheric perturbations in a relatively simple general circulation model. *Geophysical Research Letters*, **29 (7)**, 1114, doi:10.1029/2001GL014284, URL http://doi.wiley.com/10.1029/2001GL014284.

Quintanar, A., and C. Mechoso, 1995: Quasi-Stationary Waves in the Southern Hemisphere. Part II: Generation Mechanisms. *Journal of Climate*, **8**, 2673–2689.

Sampe, T., H. Nakamura, A. Goto, and W. Ohfuchi, 2010: Significance of a Midlatitude SST Frontal Zone in the Formation of a Storm Track and an Eddy-Driven Westerly Jet. *Journal of Climate*, **23 (7)**, 1793–1814, doi:10.1175/2009JCLI3163.1, URL http://journals.ametsoc.org/doi/abs/10.1175/2009JCLI3163.1.

Simmonds, I., and R. Law, 1995: Associations between Antarctic katabatic flow and the upper level winter vortex. *International Journal of Climatology*, **15 (4)**, 403–421, doi:10.1002/joc.3370150405, URL http://doi.wiley.com/10.1002/joc.3370150405.

Simpkins, G. R., S. McGregor, A. S. Taschetto, L. M. Ciasto, and M. H. England, 2014: Tropical Connections to Climatic Change in the Extratropical Southern Hemisphere: The Role of Atlantic SST Trends. *Journal of Climate*, **27 (13)**, 4923–4936, doi:10.1175/JCLI-D-13-00615.1, URL http://journals.ametsoc.org/doi/abs/10.1175/JCLI-D-13-00615.1.

Simpson, I. R., T. Shaw, and R. Seager, 2014: A diagnosis of the seasonally and longitudinally varying mid-latitude circulation response to global warming. *Journal of the Atmospheric*

778 *Sciences*, **71**, 2489–2515, doi:10.1175/JAS-D-13-0325.1, URL http://journals.ametsoc.org/doi/
779 abs/10.1175/JAS-D-13-0325.1.

780 Singh, H. K. A., C. M. Bitz, and D. M. W. Frierson, 2016: The Global Climate Response to
781 Lowering Surface Orography of Antarctica and the Importance of Atmosphere–Ocean Cou-
782 pling. *Journal of Climate*, **29 (11)**, 4137–4153, doi:10.1175/JCLI-D-15-0442.1, URL http:
783 //journals.ametsoc.org/doi/10.1175/JCLI-D-15-0442.1.

784 Stephens, G. L., D. O'Brien, P. J. Webster, P. Pilewski, S. Kato, and J. L. Li, 2015: The albedo of
785 earth. Blackwell Publishing Ltd, 141–163 pp., doi:10.1002/2014RG000449.

786 Takaya, K., and H. Nakamura, 1997: A formulation of a wave-activity flux for stationary Rossby
787 waves on a zonally varying basic flow. *Geophysical Research Letters*, doi:10.1029/97GL03094.

788 Takaya, K., and H. Nakamura, 2001: A Formulation of a Phase-Independent Wave-Activity
789 Flux for Stationary and Migratory Quasigeostrophic Eddies on a Zonally Varying Basic Flow.
790 *Journal of the Atmospheric Sciences*, **58 (6)**, 608–627, doi:10.1175/1520-0469(2001)058⟨0608:
791 AFOAPI⟩2.0.CO;2, URL http://journals.ametsoc.org/doi/abs/10.1175/1520-0469{\%
792 }282001{\%}29058{\%}3C0608{\%}3AAFOAPI{\%}3E2.0.CO{\%}3B2.

793 Taylor, K. E., R. J. Stouffer, and G. A. Meehl, 2012: An Overview of CMIP5 and the Experi-
794 ment Design. *Bulletin of the American Meteorological Society*, **93 (4)**, 485–498, doi:10.1175/
795 BAMS-D-11-00094.1, URL http://journals.ametsoc.org/doi/abs/10.1175/BAMS-D-11-00094.
796 1.

797 Taylor, K. E., D. Williamson, and F. Zwiers, 2000: The sea surface temperature and sea-ice con-
798 centration boundary conditions for AMIP II simulations. Tech. rep.

Thomson, S. I., and G. K. Vallis, 2018: Atmospheric Response to SST Anomalies. Part I: Background-State Dependence, Teleconnections, and Local Effects in Winter. *Journal of the Atmospheric Sciences*, **75 (12)**, 4107–4124, doi:10.1175/JAS-D-17-0297.1, URL http://journals.ametsoc.org/doi/10.1175/JAS-D-17-0297.1.

Vallis, G. K., 2017: *Atmospheric and oceanic fluid dynamics: Fundamentals and large-scale circulation, second edition*. Cambridge University Press, 1–946 pp., doi:10.1017/9781107588417.

Vallis, G. K., E. P. Gerber, P. J. Kushner, and B. A. Cash, 2004: A Mechanism and Simple Dynamical Model of the North Atlantic Oscillation and Annular Modes. *Journal of the Atmospheric Sciences*, **61 (3)**, 264–280, doi:10.1175/1520-0469(2004)061⟨0264:AMASDM⟩2.0.CO;2, URL http://journals.ametsoc.org/doi/abs/10.1175/1520-0469{\%}282004{\%}29061{\%}3C0264{\%}3AAMASDM{\%}3E2.0.CO{\%}3B2.

Vallis, G. K., and Coauthors, 2018: Isca, v1.0: a framework for the global modelling of the atmospheres of Earth and other planets at varying levels of complexity. *Geoscientific Model Development*, **11 (3)**, 843–859, doi:10.5194/gmd-11-843-2018, URL https://www.geosci-model-dev.net/11/843/2018/.

van Loon, H., J. J. Taljaard, T. Sasamori, J. London, D. V. Hoyt, K. Labitzke, and C. W. Newton, 1972: *Meteorology of the Southern Hemisphere*. American Meteorological Society, doi:10.1007/978-1-935704-33-1.

Walsh, K. J., I. Simmonds, and M. Collier, 2000: Sigma-coordinate calculation of topographically forced baroclinicity around Antarctica. *Dynamics of Atmospheres and Oceans*, **33 (1)**, 1–29, doi:10.1016/S0377-0265(00)00054-3.

820 Wang, H., and M. Ting, 1999: Seasonal Cycle of the Climatological Stationary Waves in the
821 NCEP–NCAR Reanalysis. *Journal of the Atmospheric Sciences*, **56 (22)**, 3892–3919, doi:10.
822 1175/1520-0469(1999)056⟨3892:SCOTCS⟩2.0.CO;2.

823 Williams, L. N., S. Lee, and S.-W. Son, 2007: Dynamics of the Southern Hemisphere Spiral
824 Jet. *Journal of the Atmospheric Sciences*, **64 (2)**, 548–563, doi:10.1175/JAS3939.1, URL http:
825 //journals.ametsoc.org/doi/abs/10.1175/JAS3939.1.

826 Woollings, T., A. Hannachi, and B. Hoskins, 2010: Variability of the North Atlantic eddy-driven
827 jet stream. *Quarterly Journal of the Royal Meteorological Society*, **136**, 856–868, doi:10.1002/
828 qj.625.

LIST OF TABLES

TABLE 1. A summary of the boundary conditions used for all experiments.

Experiment	SSTs and sea ice	Land and orography
CONTROL	Seasonally varying climatology, taken from AMIP (Taylor et al. 2000)	As in ERA-Interim
ZTS	SSTs 20N to 20S set to zonal mean with a smooth transition to 35N/S	As in CONTROL
ZMS	SSTs south of 35S set to zonal mean with a smooth transition 20S to 35S	As in CONTROL
NSI	Sea ice edge moved back to the edge of land	As in CONTROL
NOROG	As in CONTROL	Antarctic orography removed
ZTS_NOROG	As in ZTS	Antarctic orography removed
COOL	As in CONTROL	Antarctic orography removed

LIST OF FIGURES

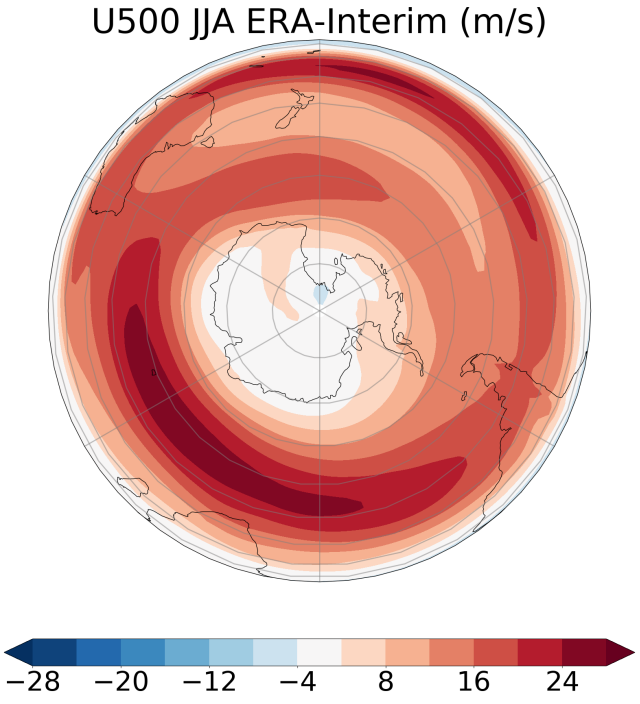

FIG. 1. ERA-Interim mean zonal wind on the 500hPa level for the SH during JJA.

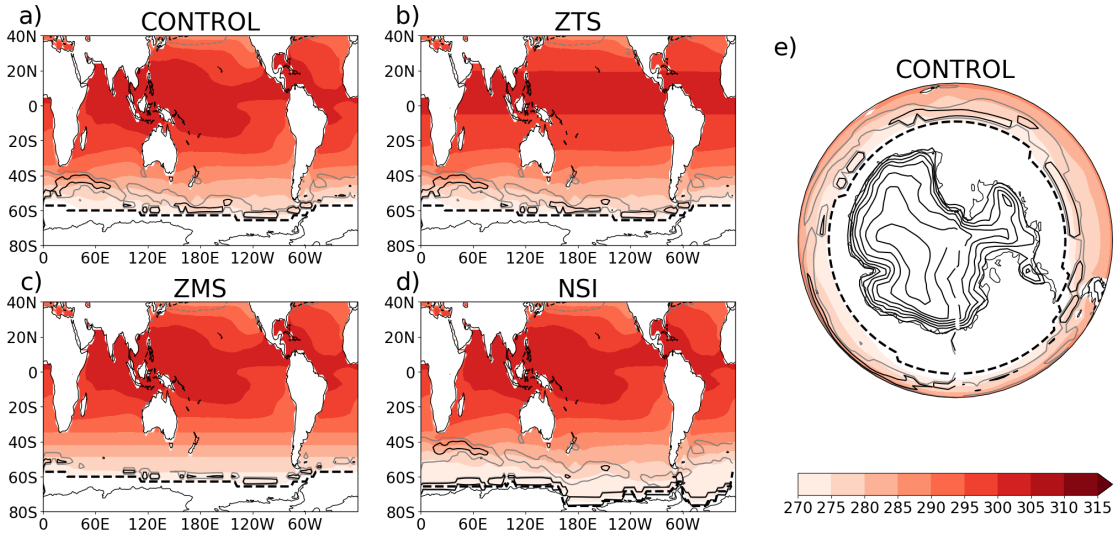

FIG. 2. A comparison of boundary conditions used in experiments. JJA SSTs are shown by colours for the a) CONTROL, b) ZTS, c) ZMS and d) NSI runs, alongside the 50% sea ice edge indicated by a dashed, black line. Meridional SST gradients above $5 \times 10^{-7} Km^{-1}$ and $8 \times 10^{-7} Km^{-1}$ are indicated by solid grey and black curves respectively. Panel e) shows topography over Antarctica in the CONTROL run with contours drawn every 500m starting at 500m.

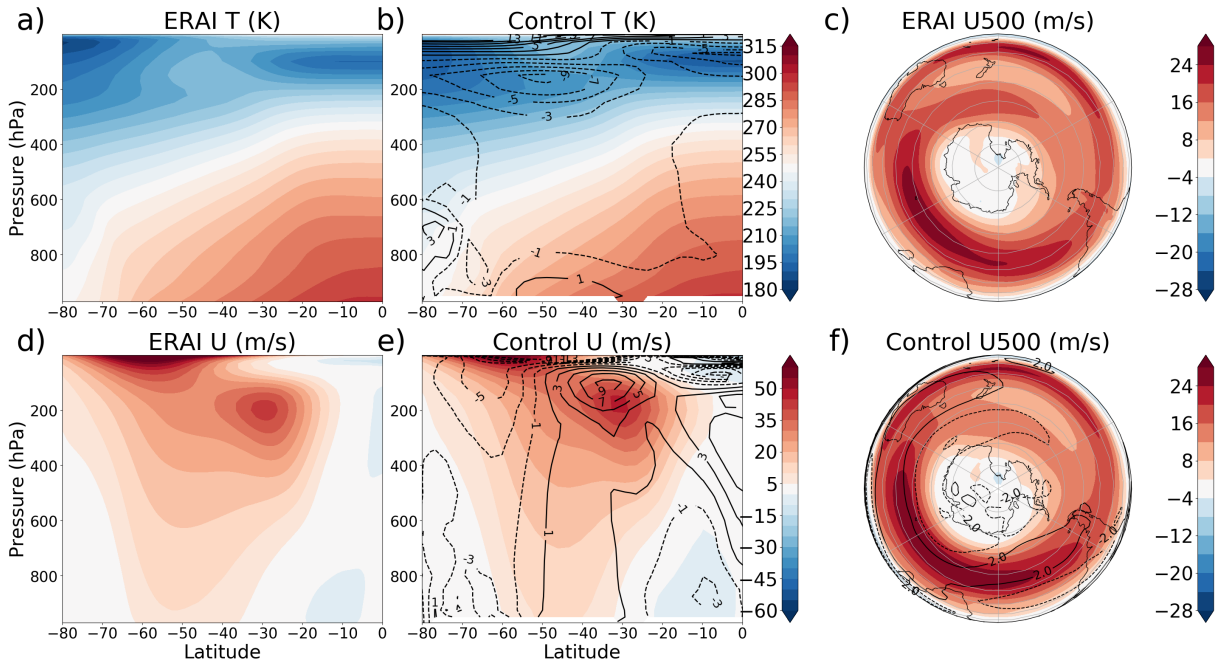

FIG. 3. Comparison of wintertime (JJA) zonal wind and temperature in the CONTROL run with ERA-Interim (1979-2014). Zonal mean temperature is shown by colours for a) ERA-Interim and b) CONTROL with contours in b) indicating the model bias, CONTROL - ERA-Interim (contour interval $2K$, beginning at $\pm 1K$). Panels d) and e) are the same as a) and b) respectively, but for zonal mean zonal wind (bias contour interval of $2ms^{-1}$, beginning at $\pm 1ms^{-1}$). The 500hPa zonal wind is shown for c) ERA-Interim and f) CONTROL with contours again showing the bias (contour interval $2ms^{-1}$)

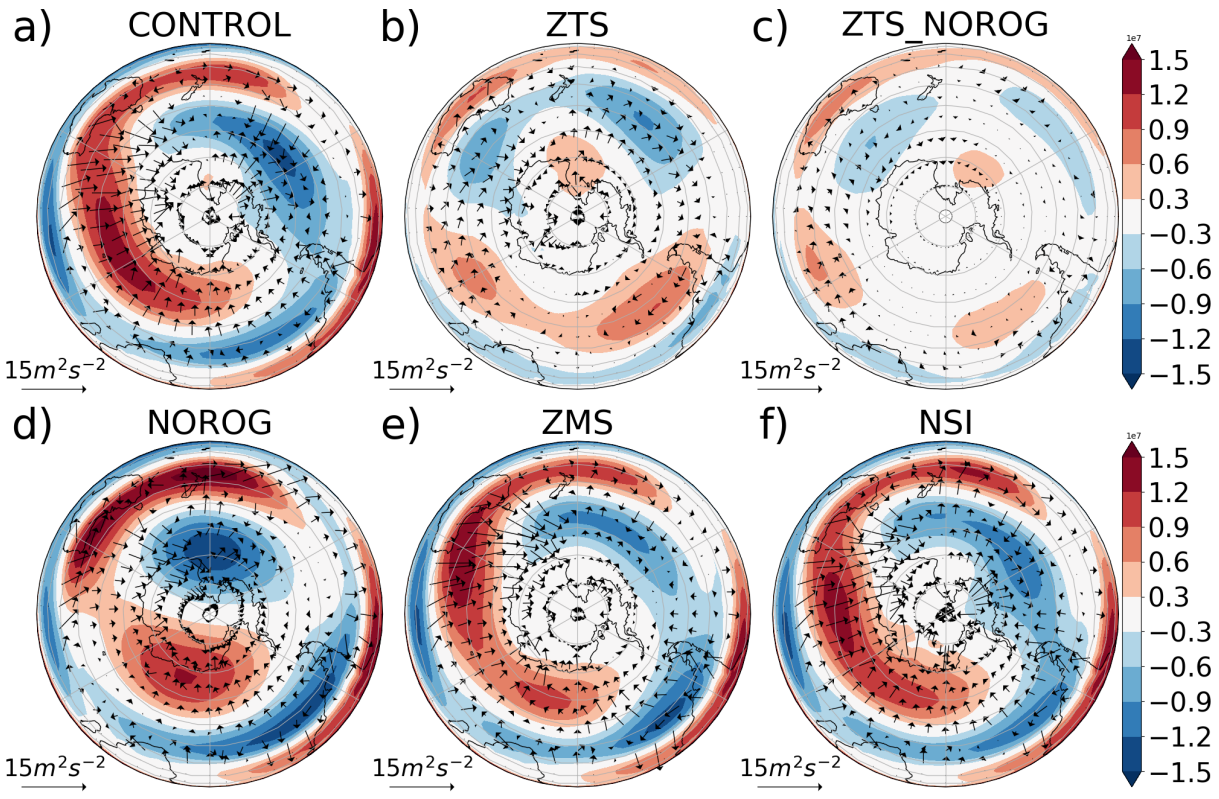

FIG. 4. Time-mean stationary waves for the different model runs during JJA. Each panel shows the 300hPa stationary eddy stream function in colours with contour interval $0.3 \times 10^{-7} m^2 s^{-1}$ alongside wave activity flux vectors on the same level. Red and blue colours indicate anomalously cyclonic and anticyclonic flow respectively.

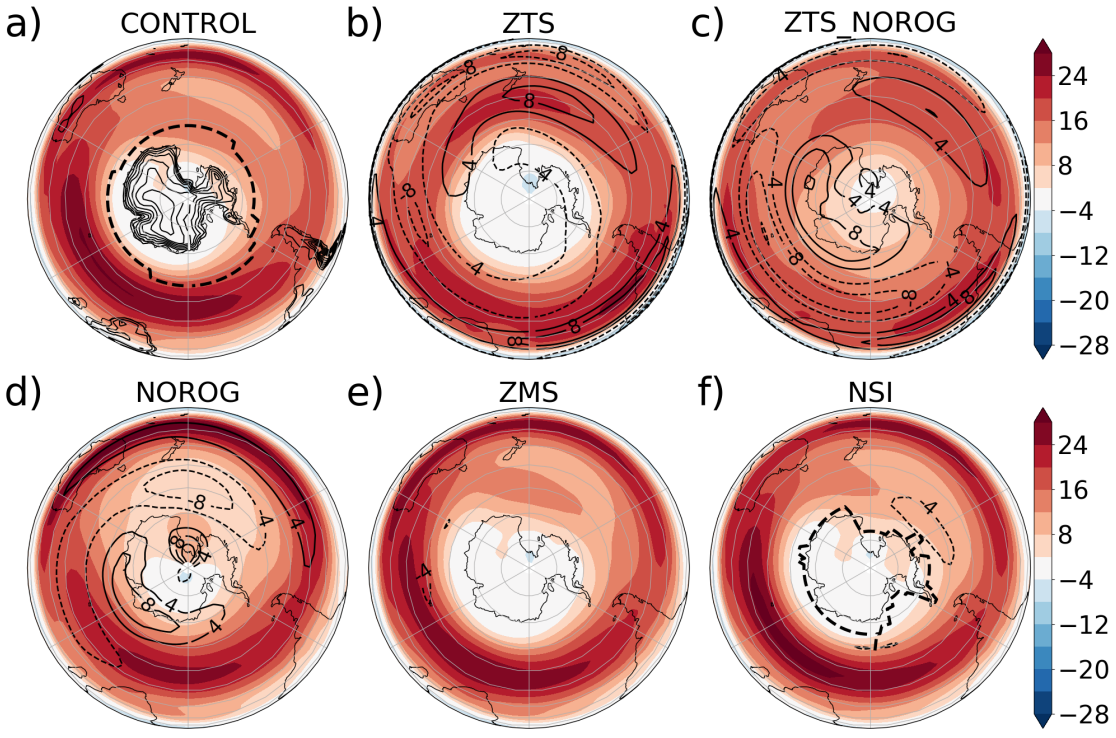

FIG. 5. Same as figure 4 but for 500hPa zonal wind. All panels show the climatology for the given run in colours and panels b) - f) show the climatology minus the CONTROL run in contours, with contour interval $4ms^{-1}$. Panel a) shows the 50% sea ice edge and topography (contoured every 500m) and f) the 50% sea ice edge for their respective runs.

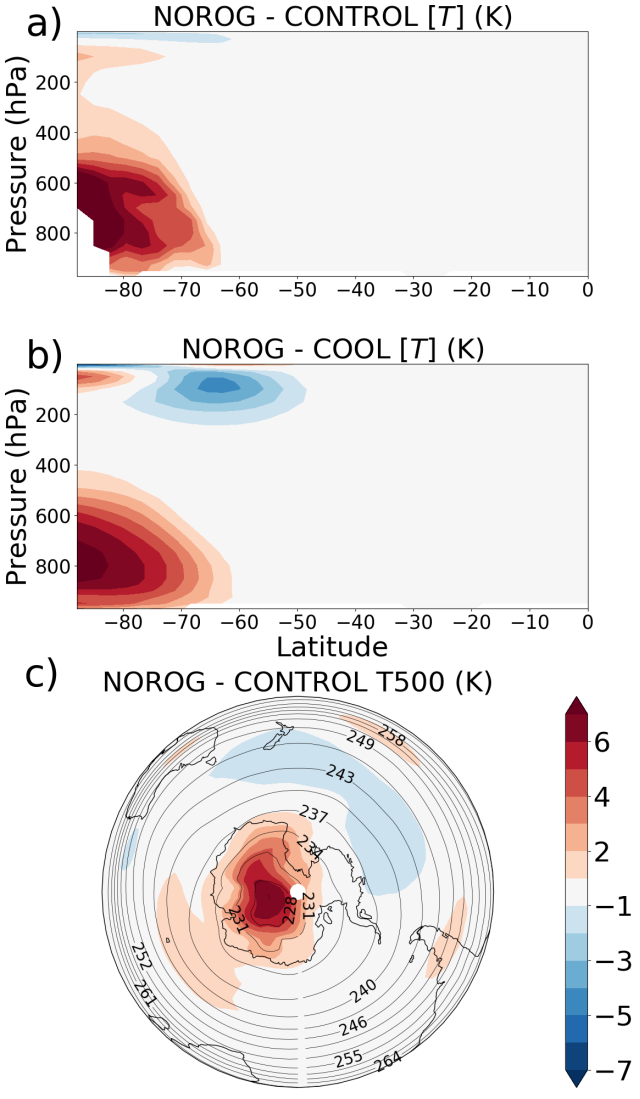

909 FIG. 6. Temperature differences between the CONTROL, NOROG and COOL runs in JJA. The zonal mean
910 temperature difference is shown for a) NOROG - CONTROL and b) NOROG - COOL, and in c) temperature
911 difference on the 500hPa level is shown for NOROG - CONTROL. In c), contours indicate the CONTROL
912 climatology values, with contour interval 3K.

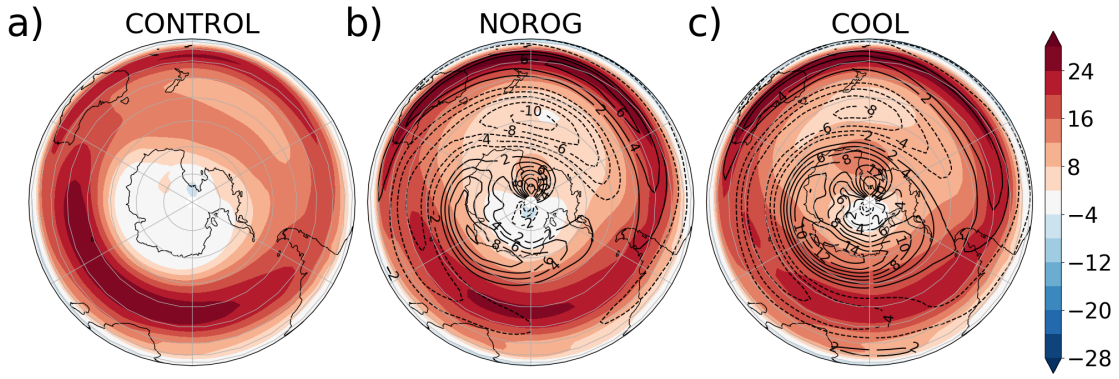

FIG. 7. 500hPa zonal wind in the run with cooling imposed. The climatology is shown by colours for a) CONTROL, b) NOROG and c) COOL, and in b) and c) contours indicate the difference from CONTROL with contour interval $2ms^{-1}$.

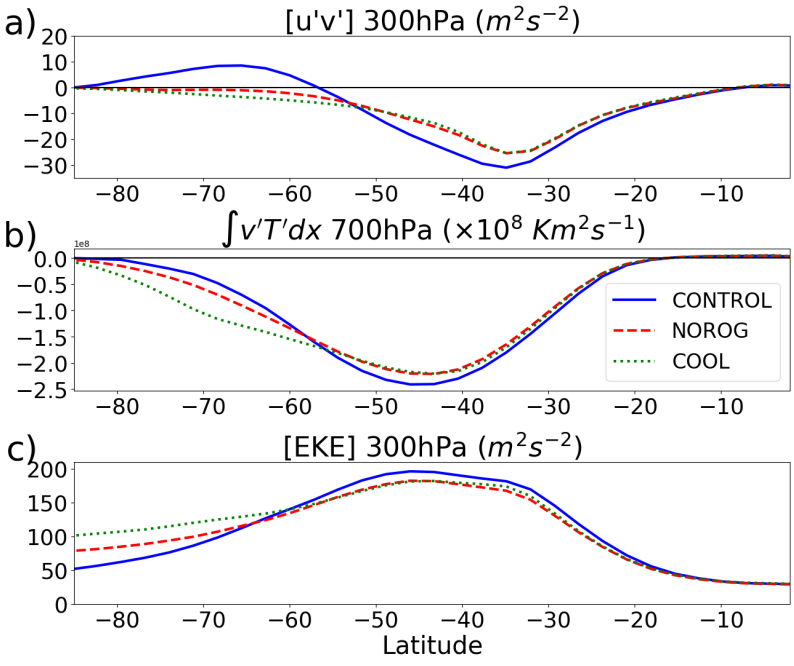

FIG. 8. Zonal mean eddy statistics for CONTROL (solid), NOROG (dashed) and COOL (dotted). a) Zonal mean transient northward eddy momentum flux, $u'v'$, at 300hPa, b) zonally integrated transient northward eddy heat flux, $v'T'$, at 700hPa and c) transient eddy kinetic energy, $u'^2 + v'^2$, at 300hPa. In b), $v'T'$ is undefined under orography, hence $v'T'$ is integrated over all valid longitudes to show total transient eddy heat transport.

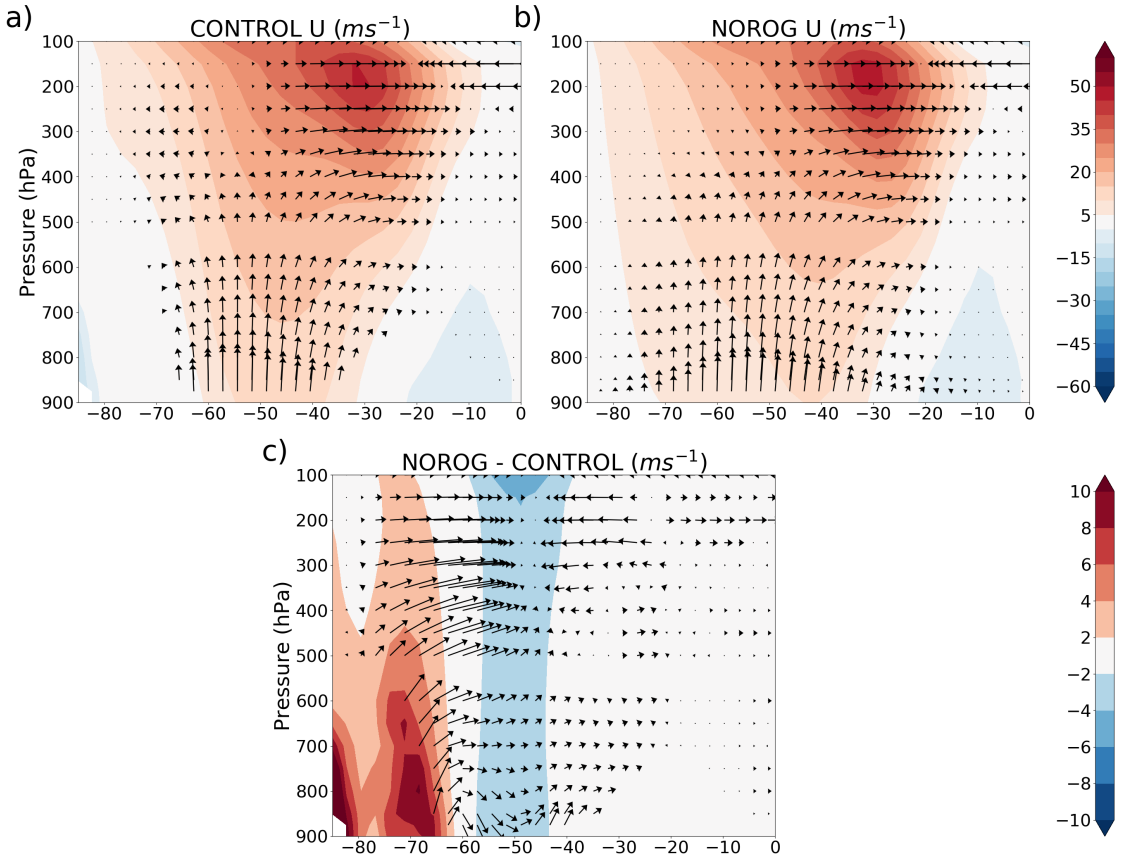

920 FIG. 9. EP flux vectors and zonal mean zonal wind for a) CONTROL b) NOROG and c) NOROG - CON-
921 TROL. EP flux vectors are not plotted in regions of significant orography.

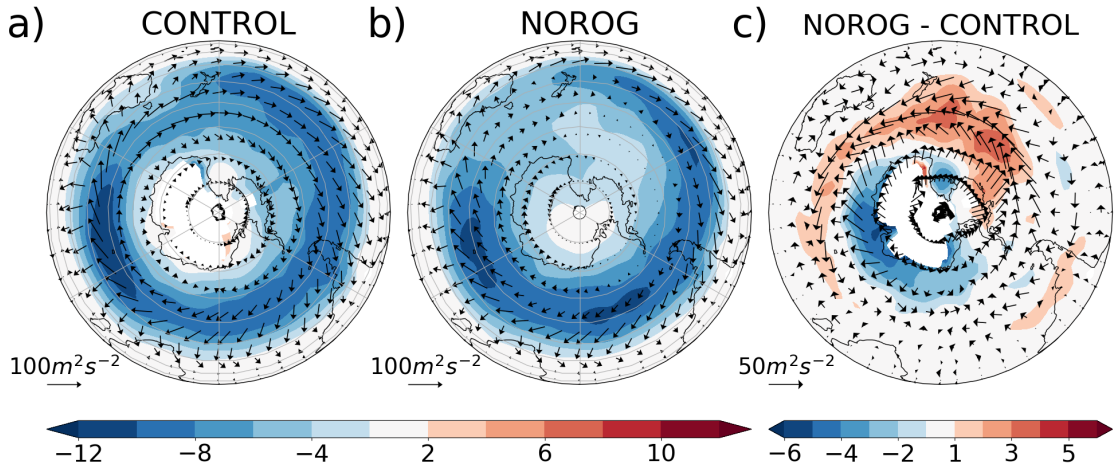

922 FIG. 10. Horizontal 300hPa E vectors and 700hPa transient eddy heat flux, $v'T'$ (colours) for a) CONTROL,
923 b) NOROG and c) NOROG - CONTROL. Transient eddy heat flux has units Kms^{-1}. As before, primes indicate
924 filtering with a 10 day high pass filter.

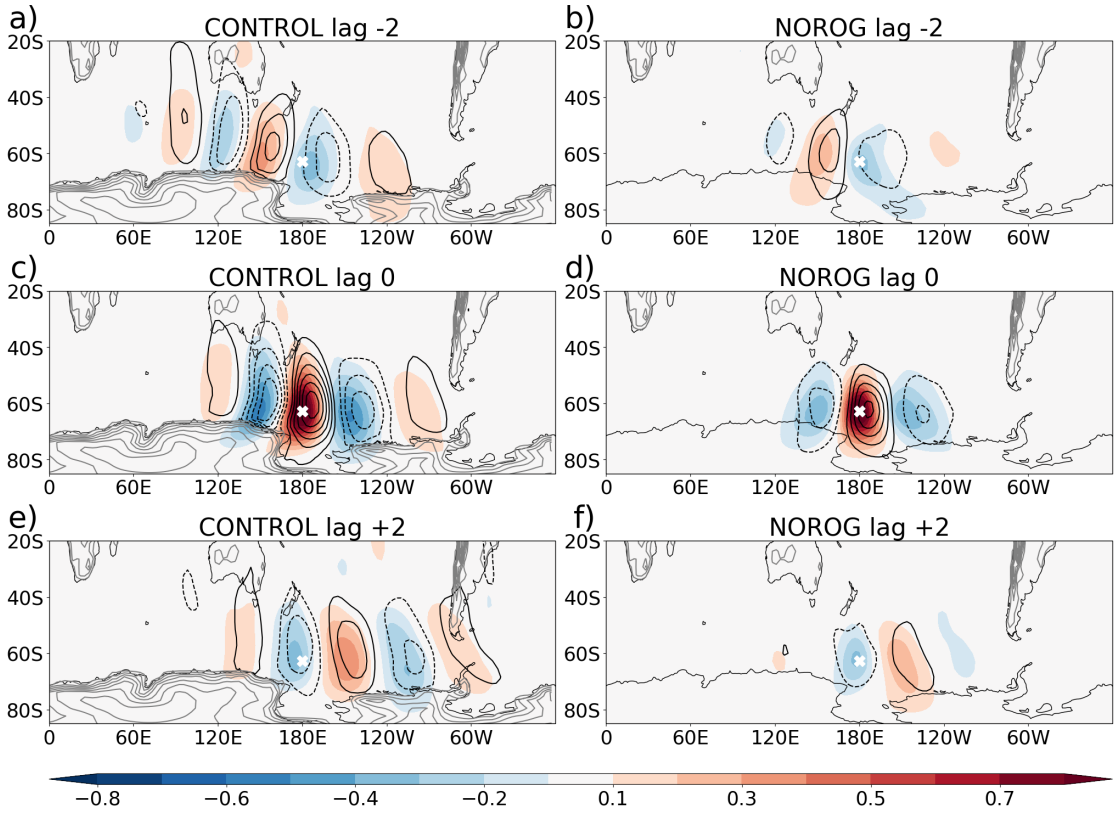

925 FIG. 11. Lagged correlations of meridional wind, as described in the text. Correlations of 300hPa meridional
926 wind at the point 180E, 62S (denoted by a cross), with 300hPa wind (colours) and 850hPa wind (contours) are
927 shown in all panels. In both cases the contour interval is 0.1. Topographic contours are also displayed in light
928 grey with contours every 500m, beginning at 500m.

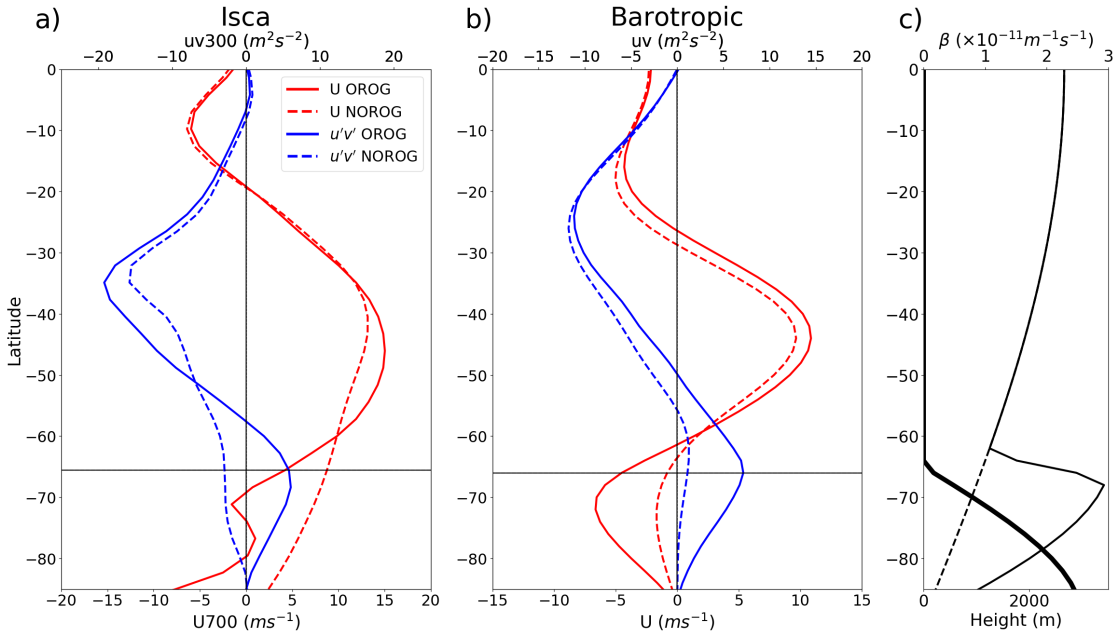

FIG. 12. Zonal mean momentum flux (blue) and zonal mean zonal wind (red) for a) Isca and b) barotropic model runs. Runs with Antarctic orography are shown by solid curves, while runs without orography are indicated by dashed curves. In a) eddy momentum flux, $u'v'$, is shown on the 300hPa level and zonal mean zonal wind shown at 700hPa. A horizontal line in a) marks the most northward latitude of the Antarctic continent and a similar line in b) marks the edge of the orography. Finally in c), orographic height in the barotropic model is shown by the thick curve and β is plotted as a function of latitude (dashed) with an estimation of the effective 'orographic β' (solid). The orographic β term is a function of vorticity so the time-mean value is shown.

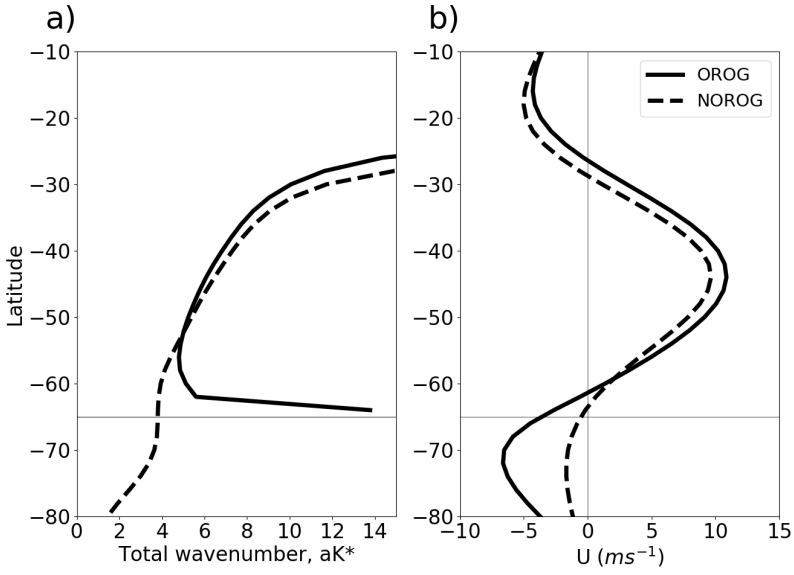

936 FIG. 13. a) Total wavenumber and b) zonal wind in the barotropic model runs. A horizontal line at 65S
937 indicates the beginning of the bottom orography.

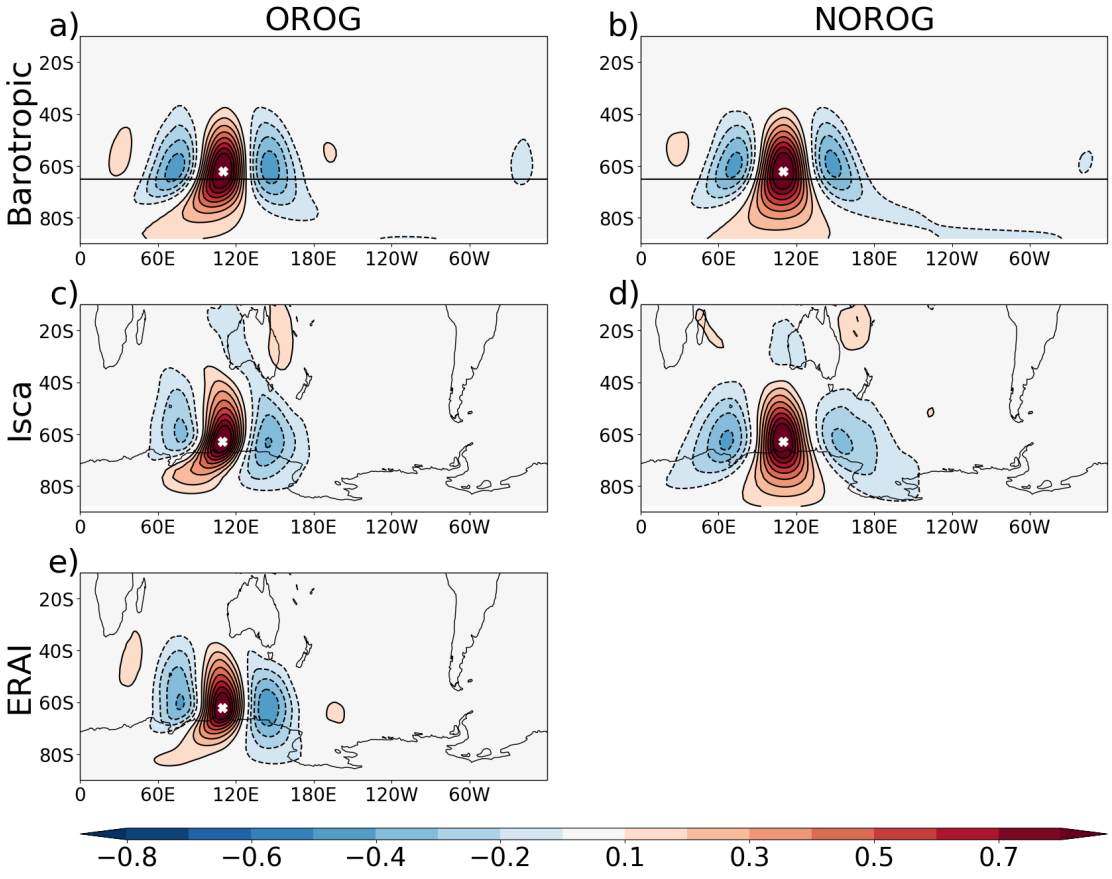

938 FIG. 14. 300hPa meridional wind correlation maps as in figure 11 but for ERA-Interim, barotropic model
939 runs and Isca runs and using the base-point, 110E, 62S (marked by a white cross).